PINHOLE X-RAY/CORONAGRAPH OPTICAL SYSTEMS CONCEPT DEFINITION STUDY

Final Report
Contract Number NAS8-33697
September 12, 1980

T.F. Zehnpfennig
S.A. Rappaport
R.B. Wattson

Visidyne, Inc.
5 Corporate Place
So. Bedford Street
Burlington, MA 01803

Prepared for:
George C. Marshall Space Flight Center
Marshall Space Flight Center, Alabama 35812

VISIDYNE
5 CORPORATE PLACE ■ SOUTH BEDFORD STREET ■ BURLINGTON, MASSACHUSETTS 01803
(617)273-2820

TABLE OF CONTENTS

1.0 Introduction and Conclusions

This is the final report for Contract NAS8-33697, Pinhole X-ray/Coronagraph Satellite Optical Systems Concept Definition Study. The Pinhole X-ray/Coronagraph Concept utilizes the long baselines possible in earth orbit with the Space Transportation System (Shuttle) to produce observations of solar x-ray emission features at extremely high spatial resolution (up to 0.1 arc second) and high energy (up to 100 keV), and also white light and UV observations of the inner and outer corona at high spatial and/or spectral resolution. The feature which is common to the x-ray instruments and the coronagraph is a mask, usually called the Occulter in this study, which is located as far as is possible and practical from the instrument package (x-ray detectors and coronagraphs), and contains coded apertures of two types for the x-ray experiments and external occulting edges for the coronagraphs. In its ultimate form, the concept will involve a free-flying satellite carrying the various instruments which would station-keep with the Shuttle at ranges of up to 10 km. The large occulter would be extended from the Shuttle bay. This concept is described in detail in the NASA Five Year Plan Summary.

The present study is limited to an examination of various aspects of a more modest, preliminary version of the X-ray Pinhole/Coronagraph Concept. For this preliminary version, the instrument package will be carried in the Shuttle bay on a mounting platform such as the IPS, and will be connected to the occulter with a deployable boom such as an Astromast. Generally, the spatial resolution, stray light levels, and minimum limb observing angles improve as the boom length increases. However, the associated engineering problems also become more serious with greater boom lengths, as detailed in a companion study by Sperry Support Services (NASA MSFC Contract NAS8-33588). At this time, boom lengths in the range from 10 meters to 50 meters are under consideration.

Table 1.1 lists a set of guidelines which were used as groundrules in conducting this study. These guidelines were generally arrived at by a consensus process in discussions and meetings with various members of the Scientific Working Group and with MSFC personnel.

Section 2.0 of this report contains a system geometry study of the tradeoffs involving the boom length, the stray light diffracted into the White Light Coronagraph by the external occulter, the minimum limb observing angle,

TABLE 1.1

PRELIMINARY GROUNDRULES

Pinhole X-Ray/Coronagraph Optical Systems Concept Definition Study

Boom Length: Up to 50 meters

Pointing Accuracy: 10 arc sec.

Pointing Stability: 0.5 arc sec., maximum, over 10 second time intervals.

System is to be capable of carrying all instruments (X-ray experiment and coronagraph(s)) on any flight.

The X-ray experiment will utilize the full boom length.

Simultaneous observations with all instruments are to be possible.

Orbital Altitude: 200 nautical miles, nominal.

White Light Coronagraph Characteristics:

Field of View:	3 1/2° diameter
Resolution:	1 arc second
Minimum Limb Observing Distance:	$0.1R_{\odot}$ (design goal)
Stray Light Level:	$5x10^{-11}$ $B_{\odot}$ (design goal)
Exposure Times:	0.1 sec. to 10 sec.

Full Coronal Coverage (360° azimuth angle) is not necessary.

and the diffraction-limited spatial resolution. Because several factors, such as boom length, which enter into the system geometry study cannot be finalized at this time, the results of this part of the study have been left in parametric form and no definite conclusions are drawn. Rather, the results here are intended to serve as a guide in evaluating various future designs.

Section 3.0 is a study of the effects of other sources of stray light on the coronagraphs, such as backlighting of the occulter by sunlight reflected from the earth and from the Shuttle. The general conclusion in this section is that the effects of these sources of stray light will be minimal for both the White Light and UV Coronagraphs, assuming state-of-the-art scattering coefficients for the coronagraph optics and that the boom and the region of the occulter within the White Light Coronagraph field-of-view are diffuse black surfaces. If, however, backlighting of the occulter should for some reason become a problem, various solutions using specular black reflectors on the back surface of the occulter are described.

Section 4.0 presents a set of preliminary alignment, pointing, and aspect sensing requirements, and then examines various solar and occulter aspect sensing concepts which could be used to satisfy these requirements. The aspect sensing requirements here require fractional arc second sensativity and are complicated by the unusual requirement for sensing the position and roll orientation of the occulter. However, the conclusion is that these sensing requirements can be satisfied using a set of special sensor systems made up of conventional optical elements and detectors.

The general result of this study is that no problems were encountered whose solutions were beyond the state of the art, and, thus, that the boom-mounted Pinhole X-ray/Coronagraph Concept is feasible with regard to those areas which were examined here.

2.0 System Geometry Study

In this section, a parametric study is made of the white light coronagraph system geometry in order to clarify the tradeoffs involved in various combinations of boom length, coronagraph aperture, and occulting disk diameter. For this study, the following parameters have been chosen to be the independent variables: boom length; the coronagraph aperture; and the stray light level due to solar radiation diffracted around the external occulting disk.

The amount of light diffracted around the disk is expressed in terms of the Relative Integrated Flux S, which is the ratio of the total radiation falling on the coronagraph entrance aperture with the external disk in place to that with the disk removed. S was calculated following the formulation of Fort, Morel, and Spaak[1].

$$S=\frac{2r^2\alpha_0}{\pi a^2\beta}\,[\Psi(o)-\Psi(a)] \tag{2.1}$$

where:

$$\Psi(o)=\operatorname{arcosh}\left[1+\frac{(r-\beta D)^2}{2r\beta D}\right] \tag{2.2}$$

$$\Psi(a)=\operatorname{arcosh}\left[1+\frac{(r-\beta D)^2-a^2}{2r\beta D}\right] \tag{2.3}$$

r=radius of the external occulting disk

β=angular radius of the solar disk =16 arc min.

D=occulting-disk-to-coronagraph spacing (boom length)

[1] B. Fort, C. Morel, and G. Spaak, Astron. Astrophys. 63, 243 (1978).

a=radius of coronagraph aperture

$\alpha_0=\lambda/2\pi r$

λ=wavelength of incident radiation.

In these equations, S is a dependent variable of r, D, and a. There appeared to be no clear way to invert the equations to make S an independent variable, as desired. Consequently, a computer program called SCATTER was written to calculate tables of values of S as a function r for various combinations of D and a within the ranges of interest. In these tables, any desired combination of values of S, D, and a can be found, along with the corresponding value of the dependent variable r. A program listing of SCATTER is reproduced in Appendix A.

From a given set of values for S, D, a, and r, all of the other relevant system parameters are easily computed. The diffraction-limited resolution is equal to 0.61 λ/a. The minimum limb observing angle θ_{min} is just:

$$\theta_{min}=\frac{r-a}{D}-\beta \tag{2.4}$$

The angle θ_{mid} from the limb to the mid-line of the blur of the external occulting disk is:

$$\theta_{mid}=\frac{r}{D}-\beta \tag{2.5}$$

The angle θ_{max} from the limb to the outer edge of the blur is:

$$\theta_{max}=\frac{r+a}{D}-\beta \tag{2.6}$$

From the results of these calculations, a series of 14 plots were prepared to show the inter-relationship of the various system parameters. These plots are reproduced in Figures 2.1 through 2.14. For each of these plots, the coronagraph aperture (equal to 2a) and the Relative Integrated Flux S (stray light level) were held fixed, while the boom length was allowed to vary out to a maximum of 100 meters. Only three coronagraph apertures were considered: 25.2 cm; 12.6 cm; and 6.3 cm. These correspond to diffraction limited resolutions of 0.5 sec., 1.0 sec., and 2.0 sec., respectively, for 5000 Å radiation. Figure 2.9 is a typical plot in this series. Data at the top of this figure indicate that the plot applies to a system with a coronagraph aperture of 12.6 cm, giving a resolution of 1.0 sec. at 5000 Å, and that it was made for a fixed Relative Integrated Flux S of 1.0×10^{-4} unapodized, or 5.0×10^{-6} with an apodizing factor of 1/20. The two abcissa scales show the boom length (Disk-to-coronagraph spacing) and the corresponding occulting disk diameter, as computed by SCATTER. The two ordinate scales give the distance above the solar limb in solar radii and in arc minutes. The curve labeled "Minimum Limb Observing Distance" corresponds to the angle θ_{min}, which is the inner edge of the blur of the external occulting disk. Along this curve, the collecting area of the coronagraph objective has fallen to zero and the spatial resolution in the direction of the radius vector of the sun is fully deteriorated due to shadowing by the occulting disk. (This is indicated in the lowest box to the right of the plot). The curve labeled "Mid-blur distance" corresponds to the angle θ_{mid}, the mid-line of the blur. Along the curve, one half ($62\ cm^2$) of the collecting area is being utilized, as shown in the corresponding box on the right. The quantity λ/W (1.64 sec.) in this same box is an approximate measure of the angular resolution in the radial direction. The intersecting circles to the right of this box indicate that, along the "Mid-blur" curve, half of the coronagraph aperture (represented by the small shaded semi-circle) protrudes beyond the occulting disk (the larger, clear circle). Finally, the uppermost curve corresponds to θ_{max}, the outer edge of the blur of the occulting disk. Above this curve (in the unvignetted region), the collecting area and angular resolution of the coronagraph are fully utilized.

Figures 2.1 through 2.14 provide a quantitative picture of the interplay of the various system parameters. For instance, Figure 2.9 shows that, as the boom length increases, smaller minimum limb observing distances can be achieved, with the desired 0.1 solar radii being reached for a boom length of 35 meters. A comparison of Figures 2.6 through 2.10 shows how a given minimum limb observing distance can be reached with shorter and shorter booms if the Relative Integrated Flux is allowed to rise. A comparison of Figures 2.2, 2.7, and 2.13 shows how, for a given stray light level, observations closer to the limb can be made as the cononagraph aperture is increased. However, the width of the blur of the occulting disk also increases with increasing aperture, and the unvignetted region is shifted to higher and higher solar limb distances.

In connection with the System Geometry Study, the intensity in the diffraction pattern of the external disk was calculated for various boom lengths. Again following the formulation of Fort, Morel, and Spaak[1], the intensity I in the Fresnel diffraction pattern of a circular obstruction illuminated by a distant point source is given by:

$$I=\frac{I_0 \pi Dr(r^2+x^2)}{2\pi^2 x(r^2-x^2)^2} \qquad (2.7)$$

where x is the distance from the center of the shadow of the disk. (Here, I is the local average intensity, with the fine details of the fringe pattern deleted). This can be integrated to give the intensity E in the diffraction pattern when the illumination is from a distant disk-shaped source of solar raduis S:

$$E=\frac{E_0 r\alpha_0}{\pi S x(k^2-1)^{1/2}} \qquad (2.8)$$

where:

$$k=1+\frac{(r-x)^2-S^2D^2}{2rx} \qquad (2.9)$$

Here, E_0 is the intensity which would be observed if the occulting disk were removed. Tables of values of E were calculated for boom lengths of 20, 30, 50, and 100 meters at 5000 Å and 1216 Å using another section of the program SCATTER. The results are plotted in Figures 2.15 through 2.18. The abcissa δ in these plots is equal to $r-\beta D-x$. That is, δ is the distance measured inward from the edge of the geometric shadow of the external occulter as it would exist without diffraction effects.

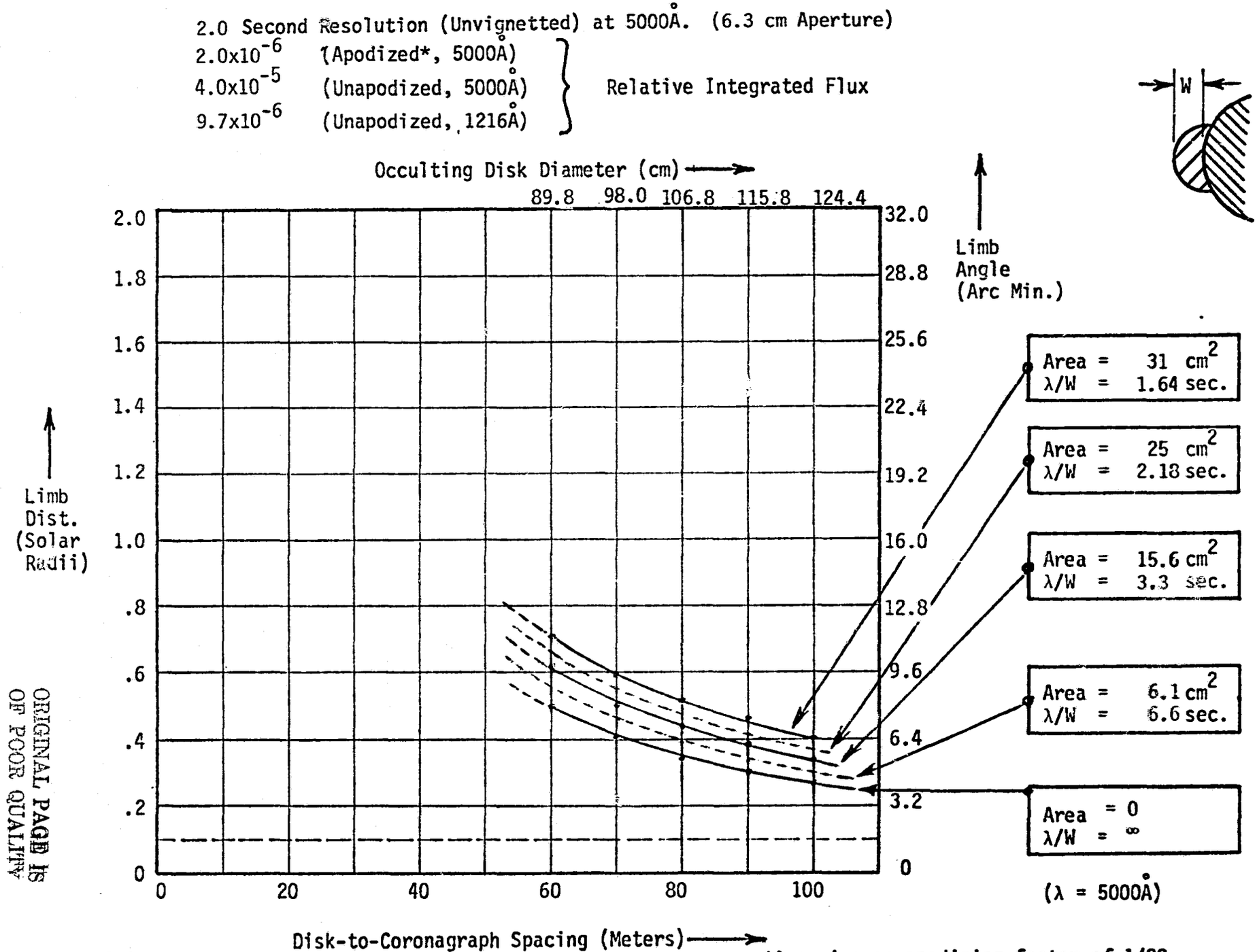

Figure 2.1

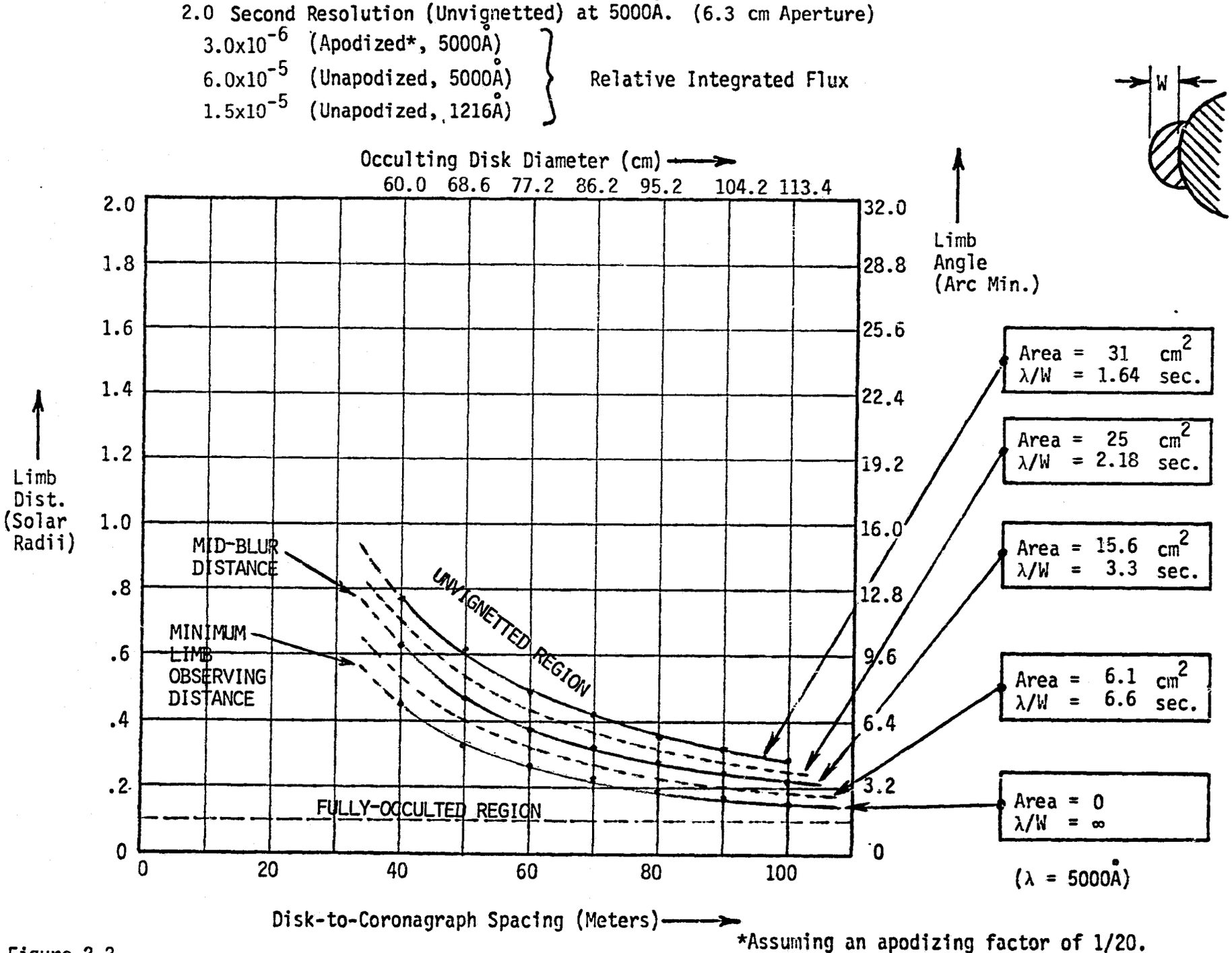

*Assuming an apodizing factor of 1/20.

Figure 2.2

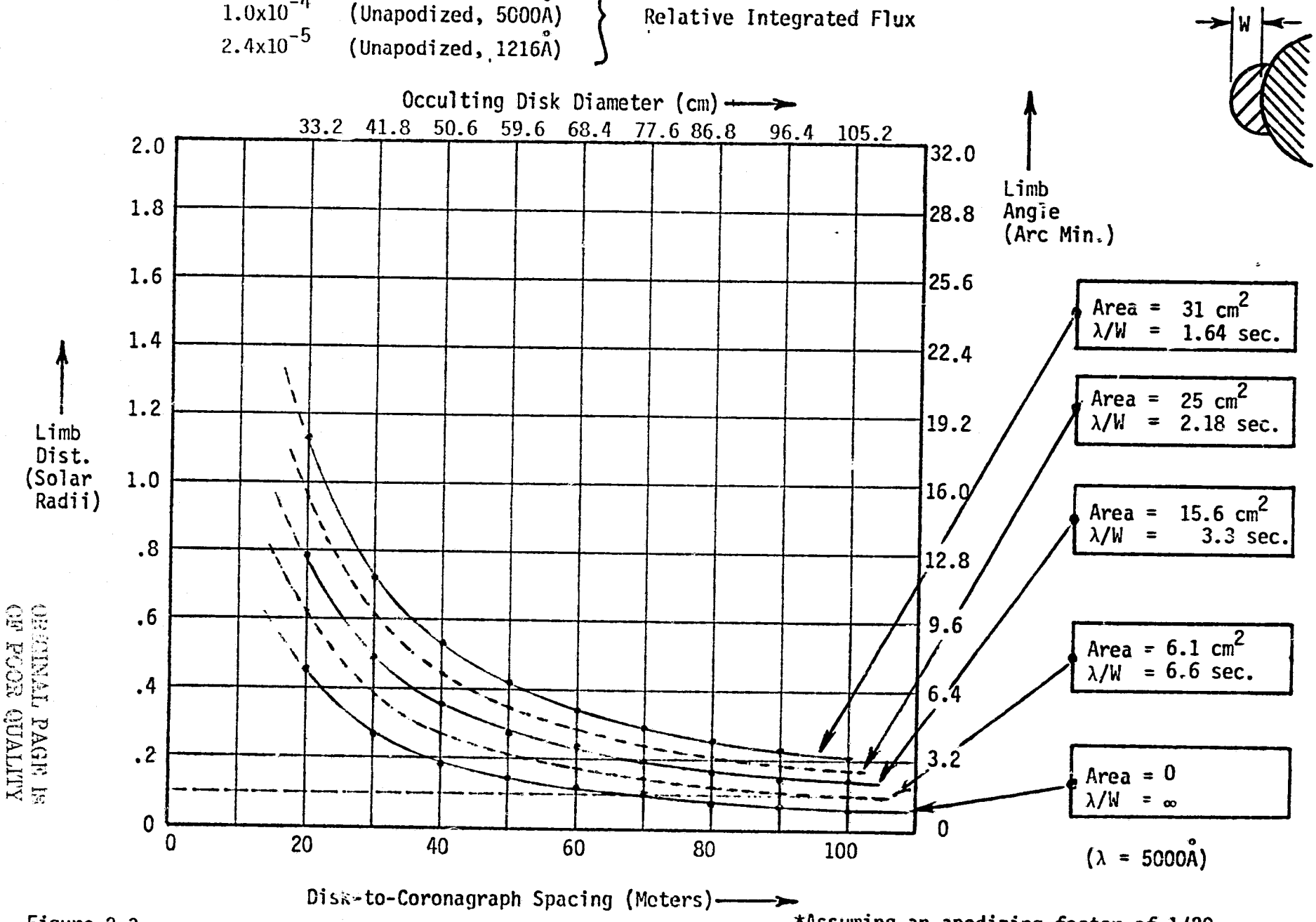

Figure 2.3

*Assuming an apodizing factor of 1/20.

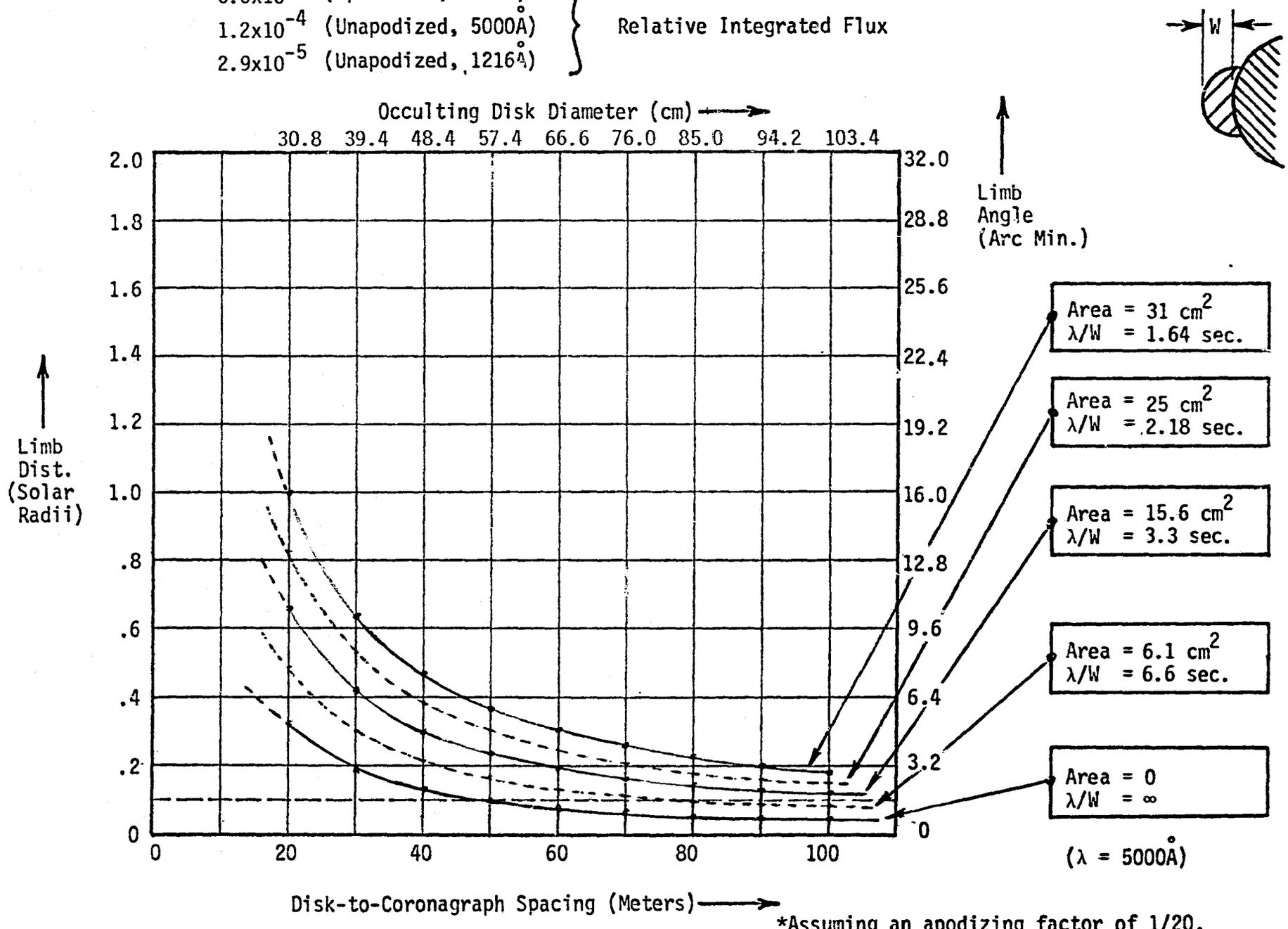
2.0 Second Resolution (Unvignetted) at 5000Å. (6.3 cm Aperture).
6.0x10^-6 (Apodized*, 5000Å)
1.2x10^-4 (Unapodized, 5000Å)
2.9x10^-5 (Unapodized, 1216Å)
Relative Integrated Flux
W
Occulting Disk Diameter (cm)
30.8 39.4 48.4 57.4 66.6 76.0 85.0 94.2 103.4
Limb Angle (Arc Min.)
Limb Dist. (Solar Radii)
2.0 1.8 1.6 1.4 1.2 1.0 .8 .6 .4 .2 0
32.0 28.8 25.6 22.4 19.2 16.0 12.8 9.6 6.4 3.2 0
0 20 40 60 80 100
Disk-to-Coronagraph Spacing (Meters)
Area = 31 cm2
λ/W = 1.64 sec.
Area = 25 cm2
λ/W = 2.18 sec.
Area = 15.6 cm2
λ/W = 3.3 sec.
Area = 6.1 cm2
λ/W = 6.6 sec.
Area = 0
λ/W = ∞
(λ = 5000Å)
*Assuming an apodizing factor of 1/20.

Figure 2.4

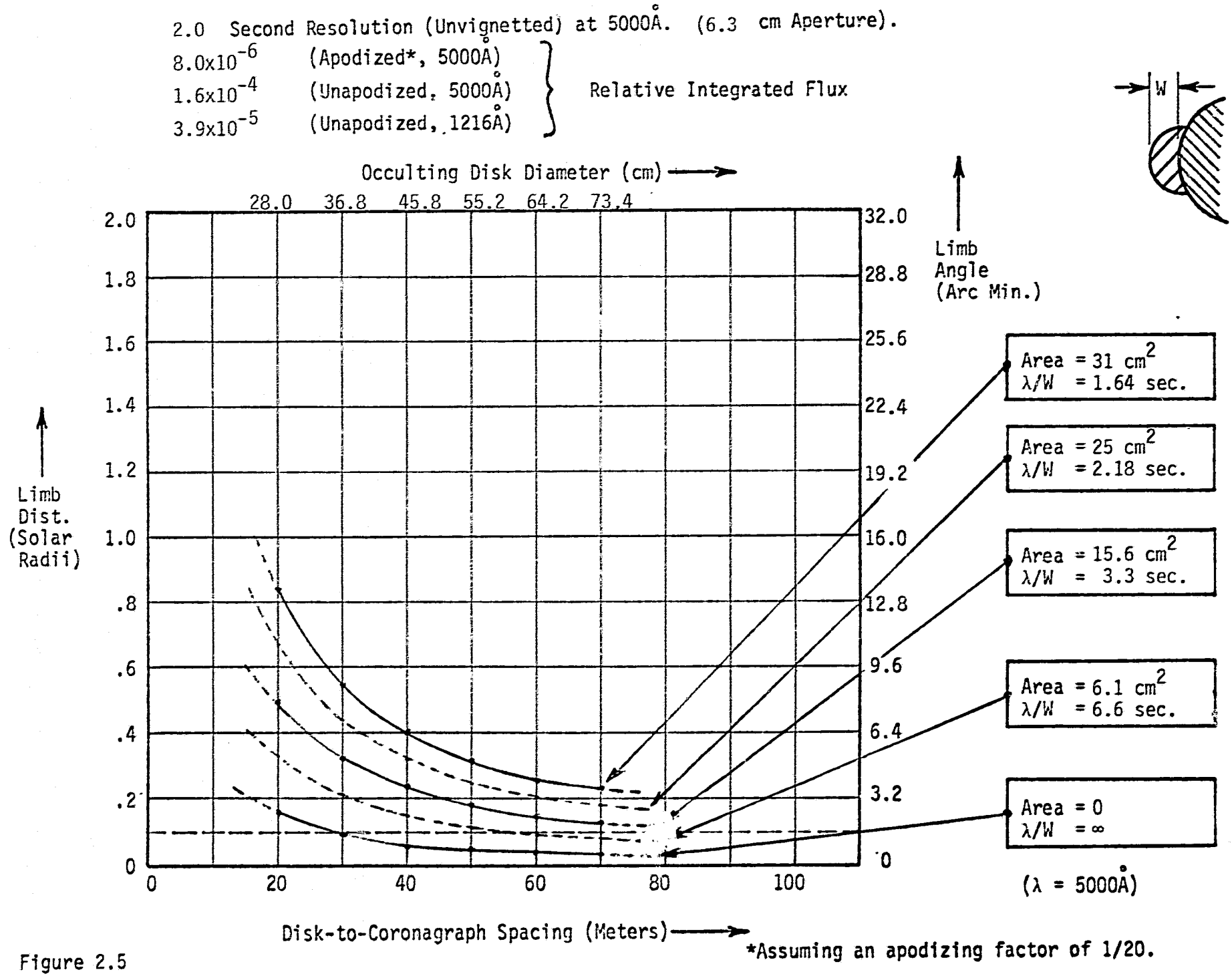
2.0 Second Resolution (Unvignetted) at 5000Å. (6.3 cm Aperture).
8.0x10^-6 (Apodized*, 5000Å)
1.6x10^-4 (Unapodized, 5000Å)
3.9x10^-5 (Unapodized, 1216Å)
Relative Integrated Flux
W
Occulting Disk Diameter (cm)
28.0 36.8 45.8 55.2 64.2 73.4
Limb Angle (Arc Min.)
Limb Dist. (Solar Radii)
2.0 1.8 1.6 1.4 1.2 1.0 .8 .6 .4 .2 0
32.0 28.8 25.6 22.4 19.2 16.0 12.8 9.6 6.4 3.2 0
0 20 40 60 80 100
Area = 31 cm2
λ/W = 1.64 sec.
Area = 25 cm2
λ/W = 2.18 sec.
Area = 15.6 cm2
λ/W = 3.3 sec.
Area = 6.1 cm2
λ/W = 6.6 sec.
Area = 0
λ/W = ∞
(λ = 5000Å)
Disk-to-Coronagraph Spacing (Meters)
*Assuming an apodizing factor of 1/20.

Figure 2.5

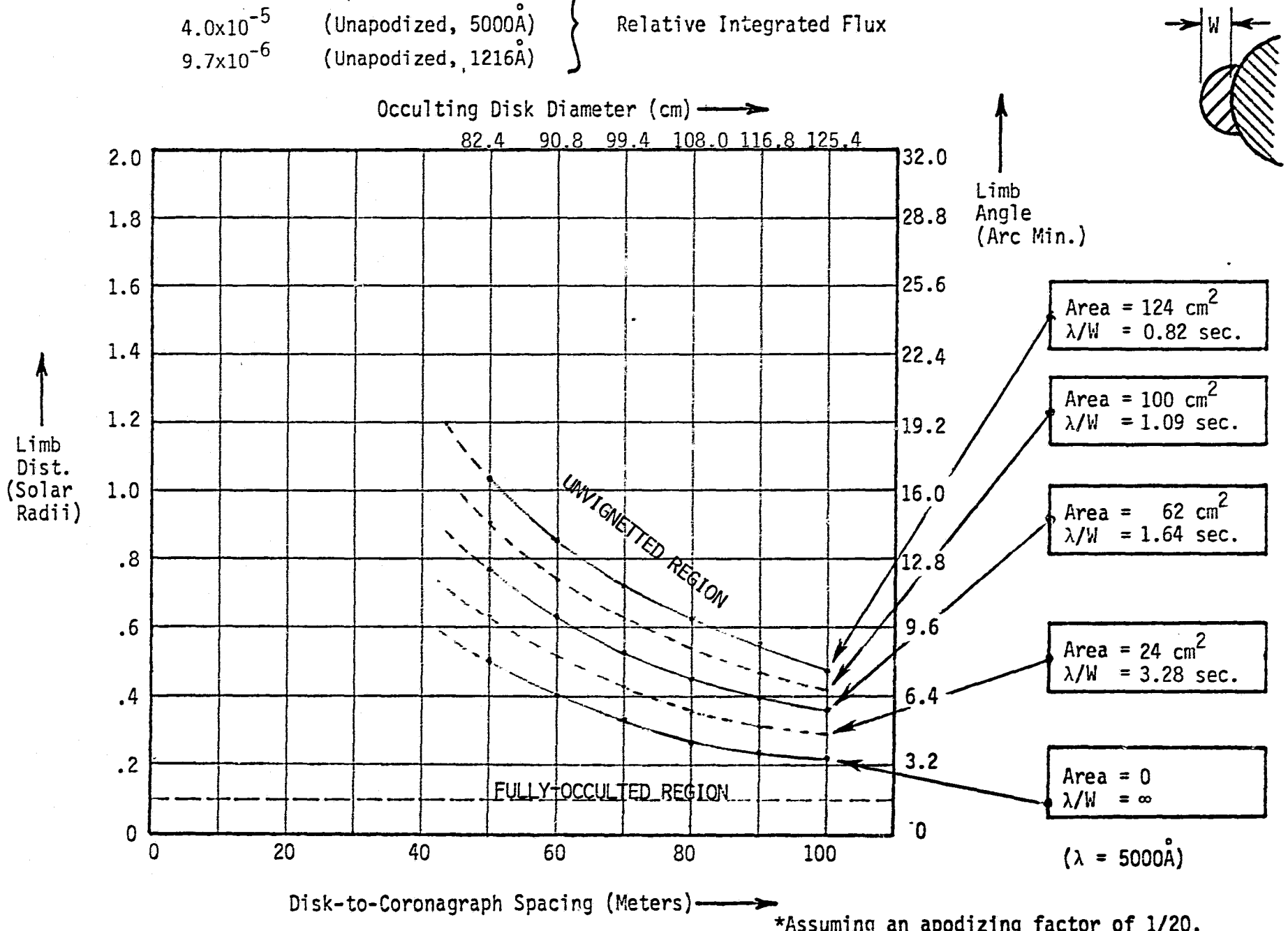
1.0 Second Resolution (Unvignetted) at 5000Å. (12.6 cm Aperture).
2.0x10^-6 Apodized*, 5000Å)
4.0x10^-5 (Unapodized, 5000Å)
9.7x10^-6 (Unapodized, 1216Å)
Relative Integrated Flux
W
Occulting Disk Diameter (cm)
82.4 90.8 99.4 108.0 116.8 125.4
Limb Angle (Arc Min.)
Limb Dist. (Solar Radii)
2.0 1.8 1.6 1.4 1.2 1.0 .8 .6 .4 .2 0
32.0 28.8 25.6 22.4 19.2 16.0 12.8 9.6 6.4 3.2 0
UNVIGNETTED REGION
FULLY-OCCULTED REGION
Area = 124 cm2
λ/W = 0.82 sec.
Area = 100 cm2
λ/W = 1.09 sec.
Area = 62 cm2
λ/W = 1.64 sec.
Area = 24 cm2
λ/W = 3.28 sec.
Area = 0
λ/W = ∞
(λ = 5000Å)
0 20 40 60 80 100
Disk-to-Coronagraph Spacing (Meters)
*Assuming an apodizing factor of 1/20.

Figure 2.6

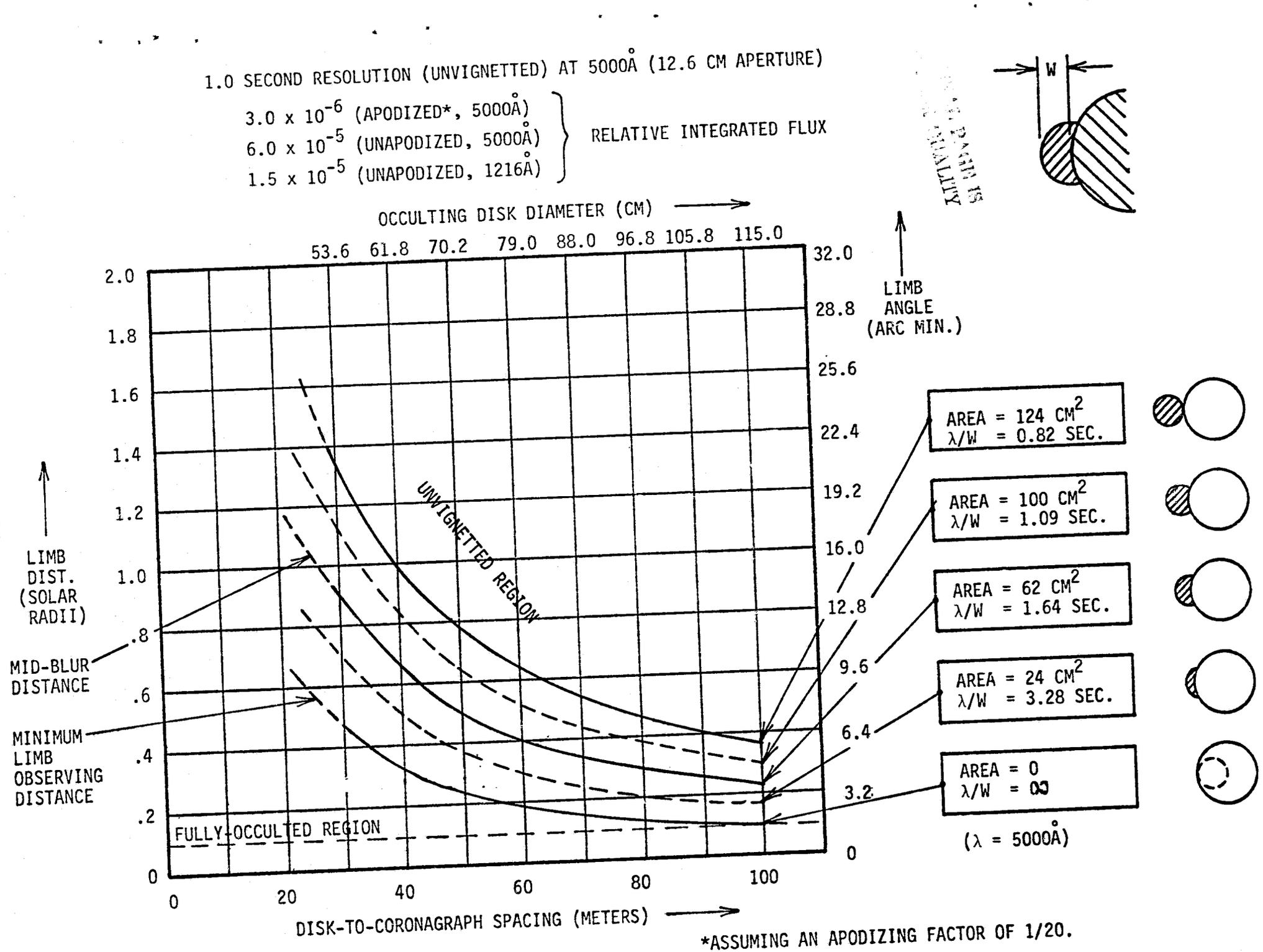
1.0 SECOND RESOLUTION (UNVIGNETTED) AT 5000Å (12.6 CM APERTURE)
3.0 x 10^-6 (APODIZED*, 5000Å)
6.0 x 10^-5 (UNAPODIZED, 5000Å)
1.5 x 10^-5 (UNAPODIZED, 1216Å)
RELATIVE INTEGRATED FLUX
W
OCCULTING DISK DIAMETER (CM)
53.6 61.8 70.2 79.0 88.0 96.8 105.8 115.0
LIMB ANGLE (ARC MIN.)
32.0 28.8 25.6 22.4 19.2 16.0 12.8 9.6 6.4 3.2 0
LIMB DIST. (SOLAR RADII)
2.0 1.8 1.6 1.4 1.2 1.0 .8 .6 .4 .2 0
MID-BLUR DISTANCE
MINIMUM LIMB OBSERVING DISTANCE
UNVIGNETTED REGION
FULLY-OCCULTED REGION
0 20 40 60 80 100
DISK-TO-CORONAGRAPH SPACING (METERS)
AREA = 124 CM2
λ/W = 0.82 SEC.
AREA = 100 CM2
λ/W = 1.09 SEC.
AREA = 62 CM2
λ/W = 1.64 SEC.
AREA = 24 CM2
λ/W = 3.28 SEC.
AREA = 0
λ/W = ∞
(λ = 5000Å)
*ASSUMING AN APODIZING FACTOR OF 1/20.

Figure 2.7

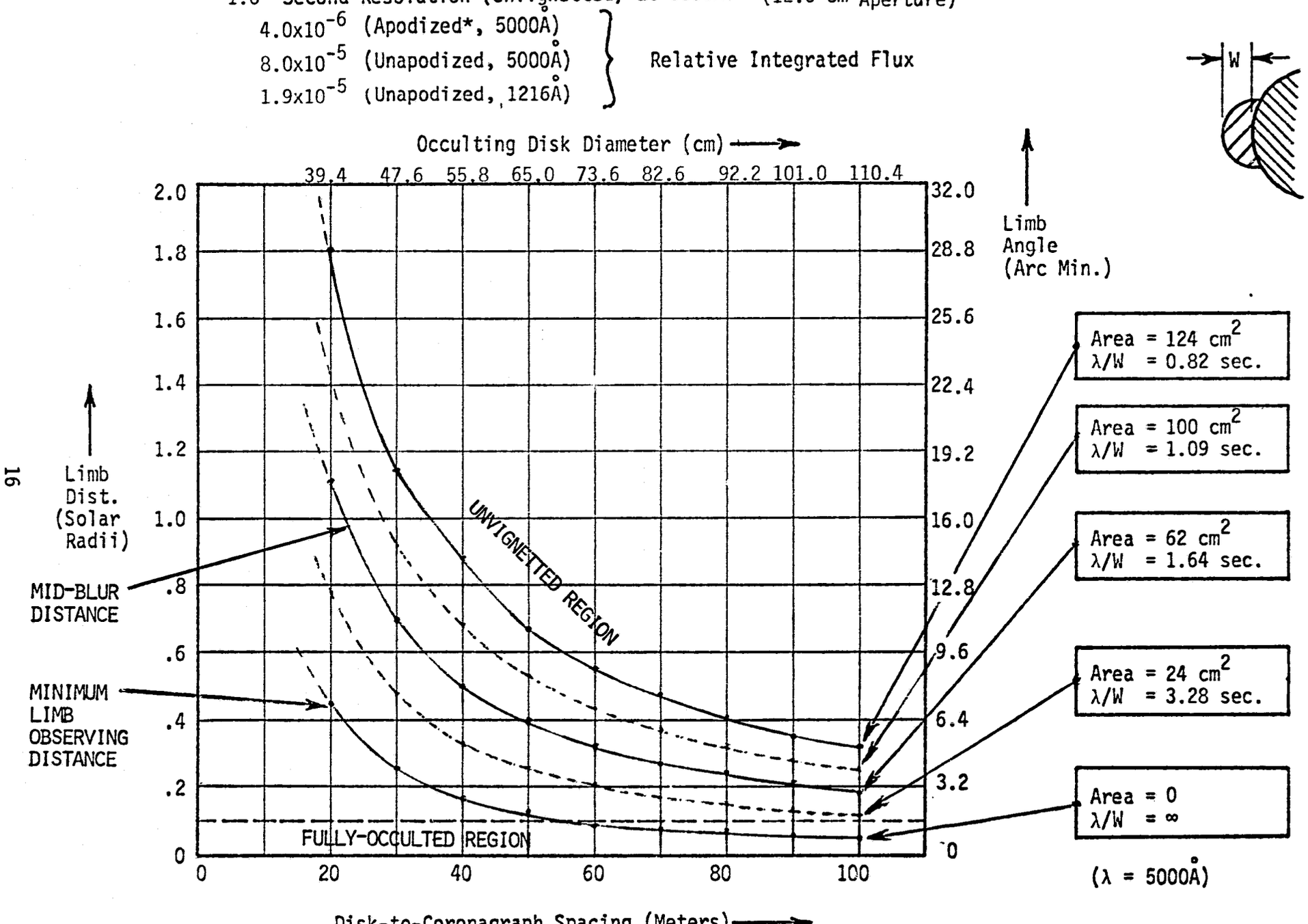
1.0 Second Resolution (Unvignetted) at 5000Å. (12.6 cm Aperture)
4.0x10^-6 (Apodized*, 5000Å)
8.0x10^-5 (Unapodized, 5000Å)
1.9x10^-5 (Unapodized, 1216Å)
Relative Integrated Flux
W
Occulting Disk Diameter (cm)
39.4 47.6 55.8 65.0 73.6 82.6 92.2 101.0 110.4
Limb Angle (Arc Min.)
Limb Dist. (Solar Radii)
MID-BLUR DISTANCE
MINIMUM LIMB OBSERVING DISTANCE
UNVIGNETTED REGION
FULLY-OCCULTED REGION
Area = 124 cm2
λ/W = 0.82 sec.
Area = 100 cm2
λ/W = 1.09 sec.
Area = 62 cm2
λ/W = 1.64 sec.
Area = 24 cm2
λ/W = 3.28 sec.
Area = 0
λ/W = ∞
(λ = 5000Å)
Disk-to-Coronagraph Spacing (Meters)
*Assuming an apodizing factor of 1/20.

Figure 2.8

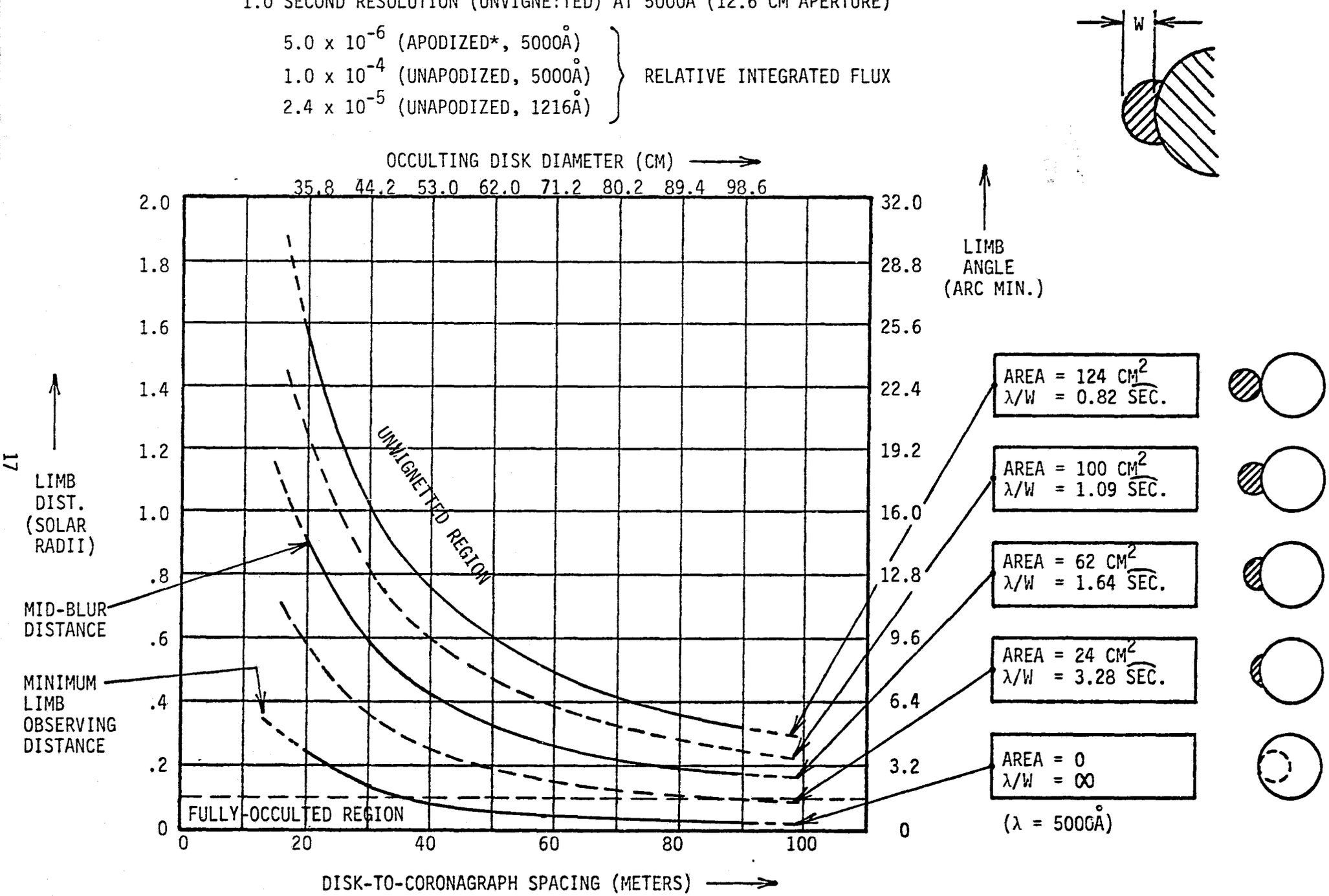

Figure 2.9

*ASSUMING AN APODIZING FACTOR OF 1/20.

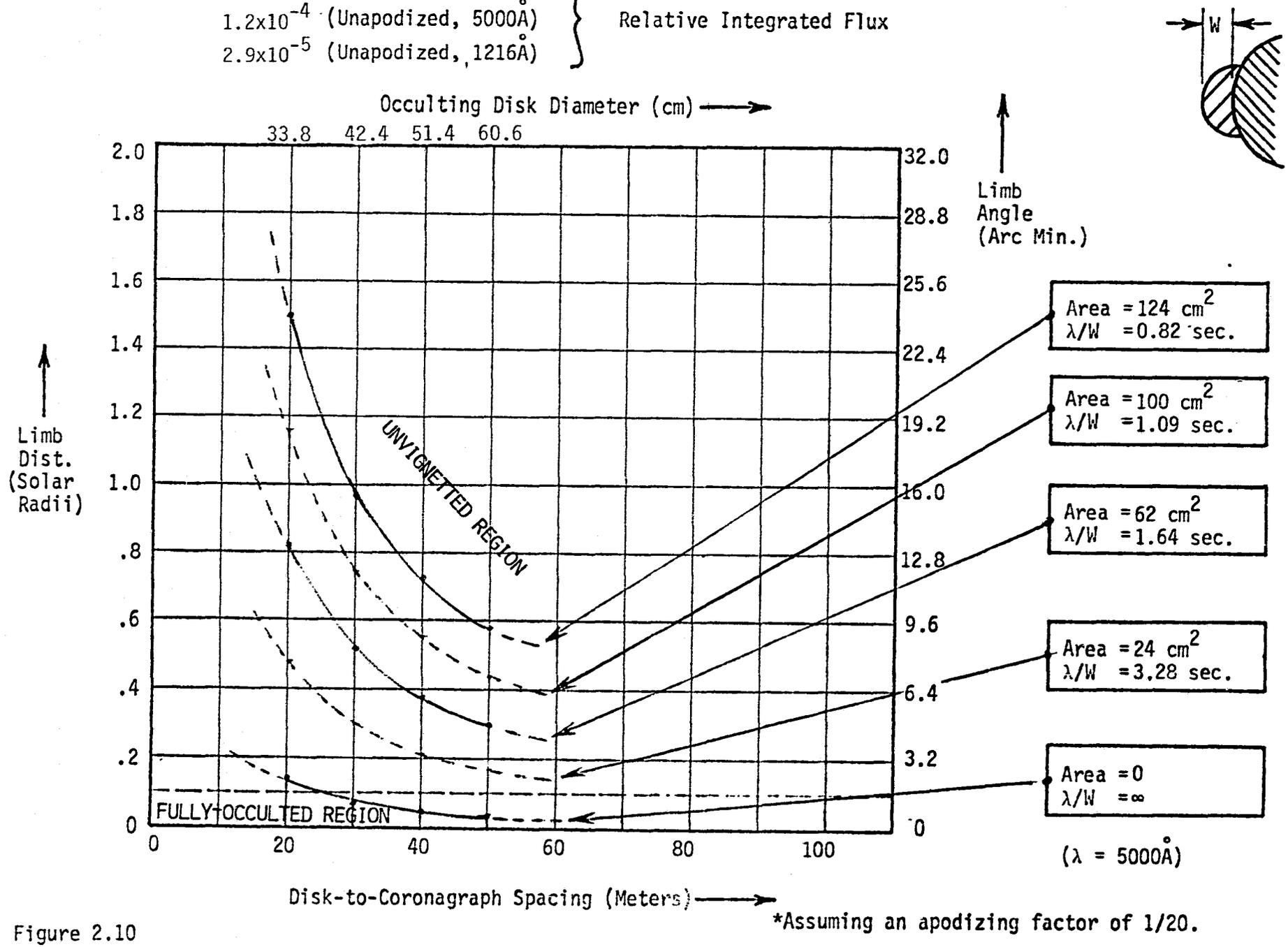

Figure 2.10

*Assuming an apodizing factor of 1/20.

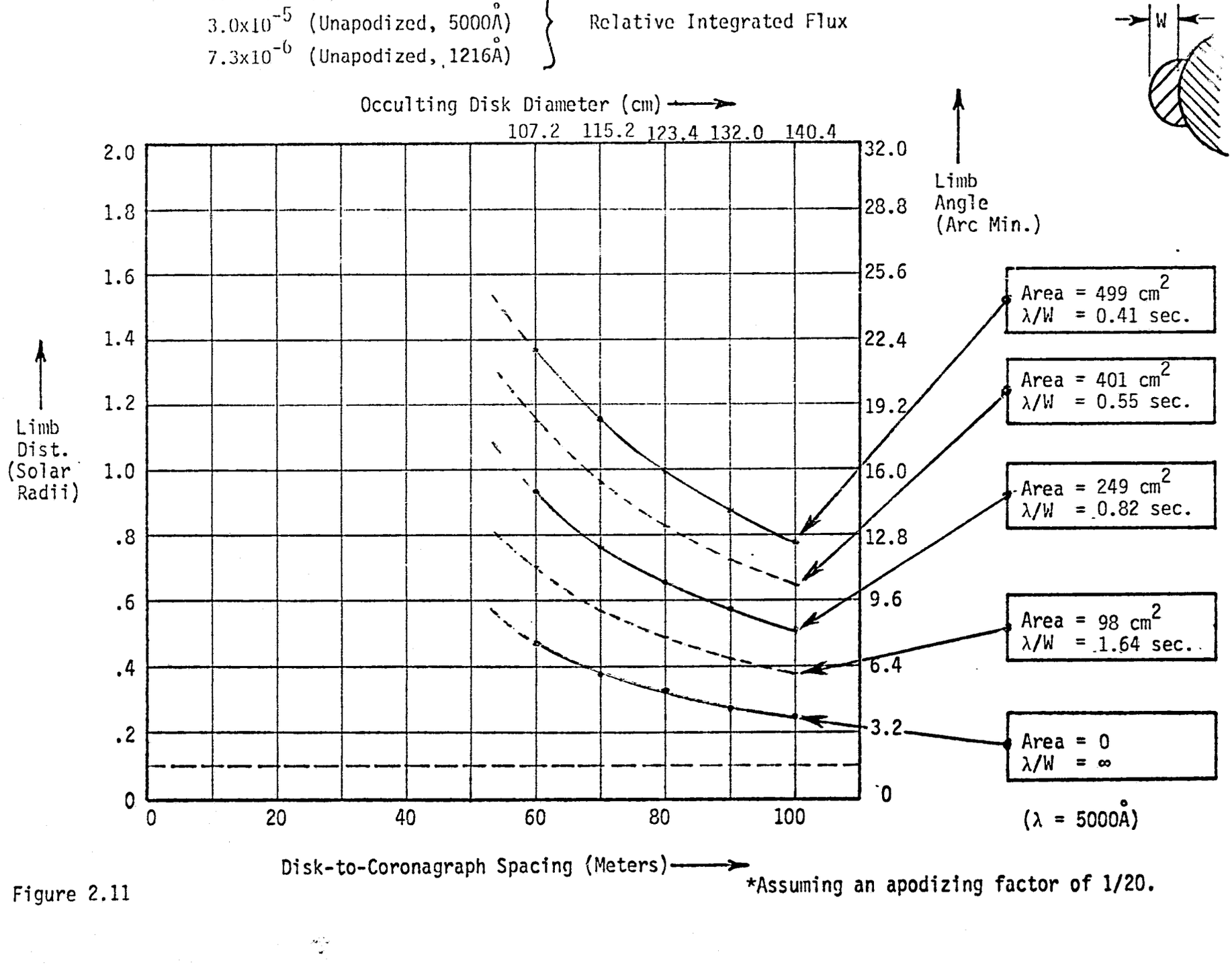

Figure 2.11

*Assuming an apodizing factor of 1/20.

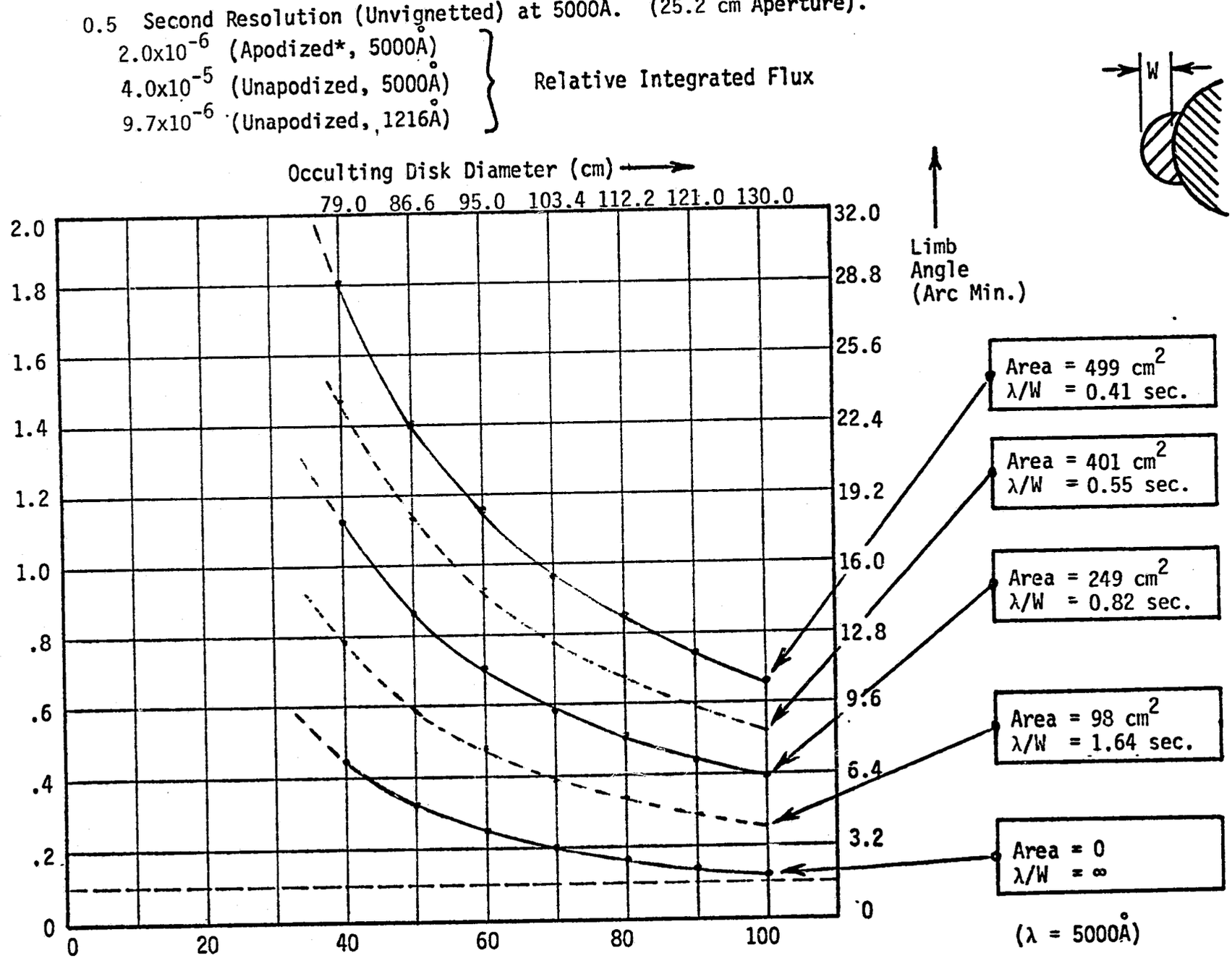

Figure 2.12

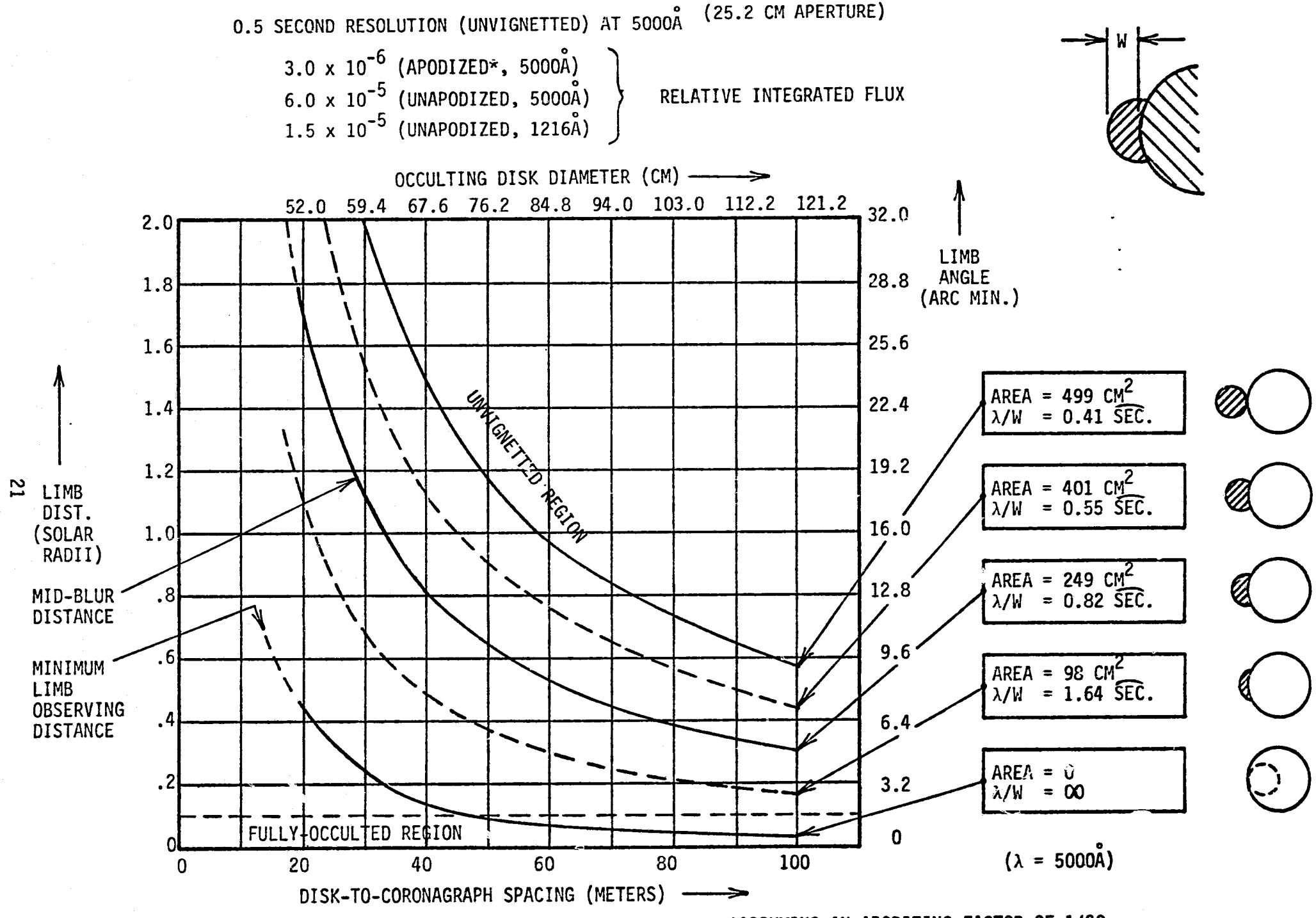
0.5 SECOND RESOLUTION (UNVIGNETTED) AT 5000Å (25.2 CM APERTURE)
3.0 x 10^-6 (APODIZED*, 5000Å)
6.0 x 10^-5 (UNAPODIZED, 5000Å)
1.5 x 10^-5 (UNAPODIZED, 1216Å)
RELATIVE INTEGRATED FLUX
W
OCCULTING DISK DIAMETER (CM)
52.0 59.4 67.6 76.2 84.8 94.0 103.0 112.2 121.2
LIMB ANGLE (ARC MIN.)
LIMB DIST. (SOLAR RADII)
MID-BLUR DISTANCE
MINIMUM LIMB OBSERVING DISTANCE
UNVIGNETTED REGION
FULLY-OCCULTED REGION
AREA = 499 CM2
λ/W = 0.41 SEC.
AREA = 401 CM2
λ/W = 0.55 SEC.
AREA = 249 CM2
λ/W = 0.82 SEC.
AREA = 98 CM2
λ/W = 1.64 SEC.
AREA = 0
λ/W = ∞
(λ = 5000Å)
DISK-TO-CORONAGRAPH SPACING (METERS)
*ASSUMING AN APODIZING FACTOR OF 1/20.

Figure 2.13

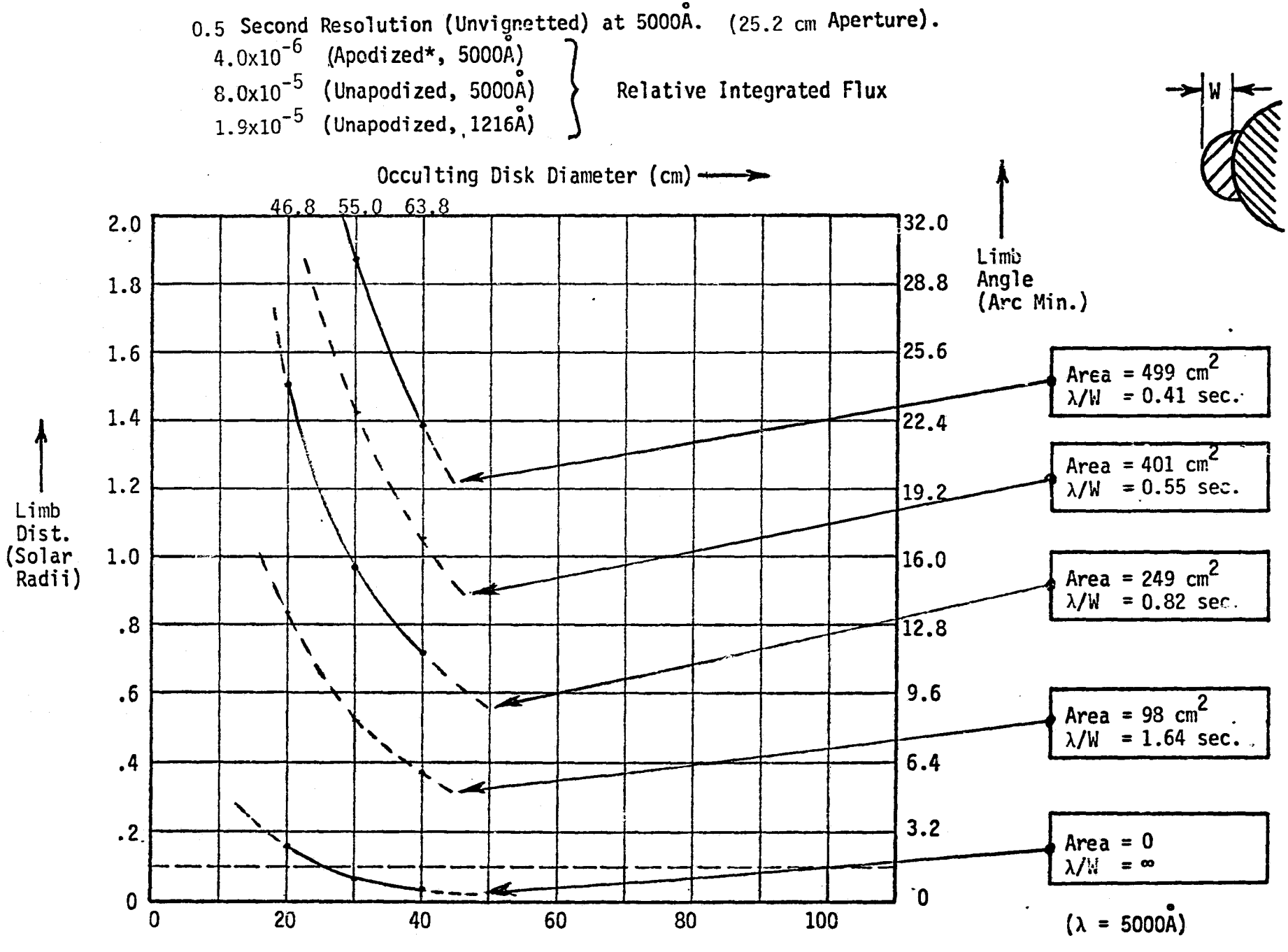

Figure 2.14

*Assuming an apodizing factor of 1/20.

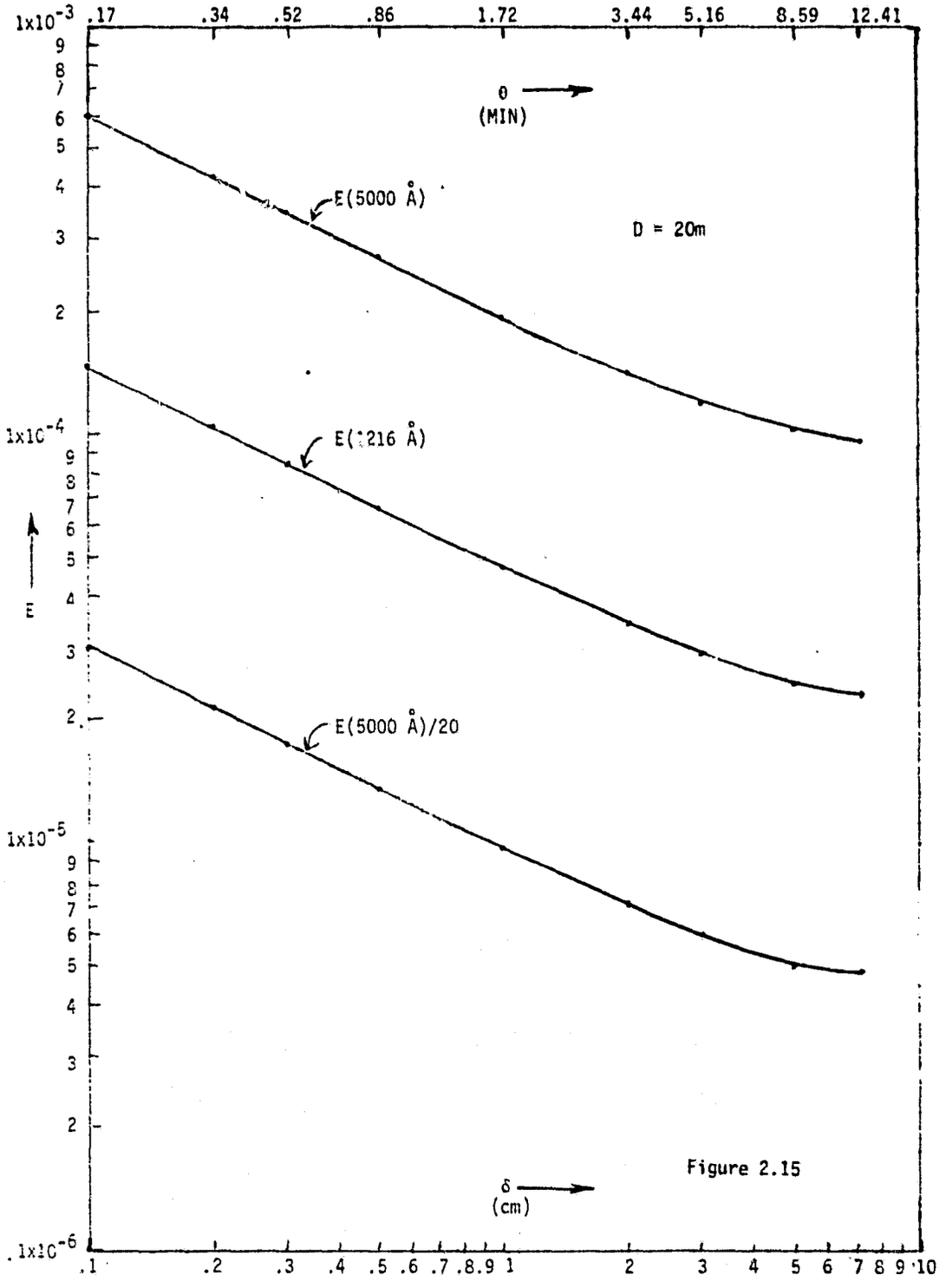
1x10-3
.17
.34
.52
.86
1.72
3.44
5.16
8.59
12.41
θ
(MIN)
E(5000 Å)
D = 20m
1x10-4
E(1216 Å)
E
E(5000 Å)/20
1x10-5
1x10-6
.1
.2
.3
.4
.5
.6
.7
.8
.9
1
2
3
4
5
6
7
8
9
10
δ
(cm)

Figure 2.15

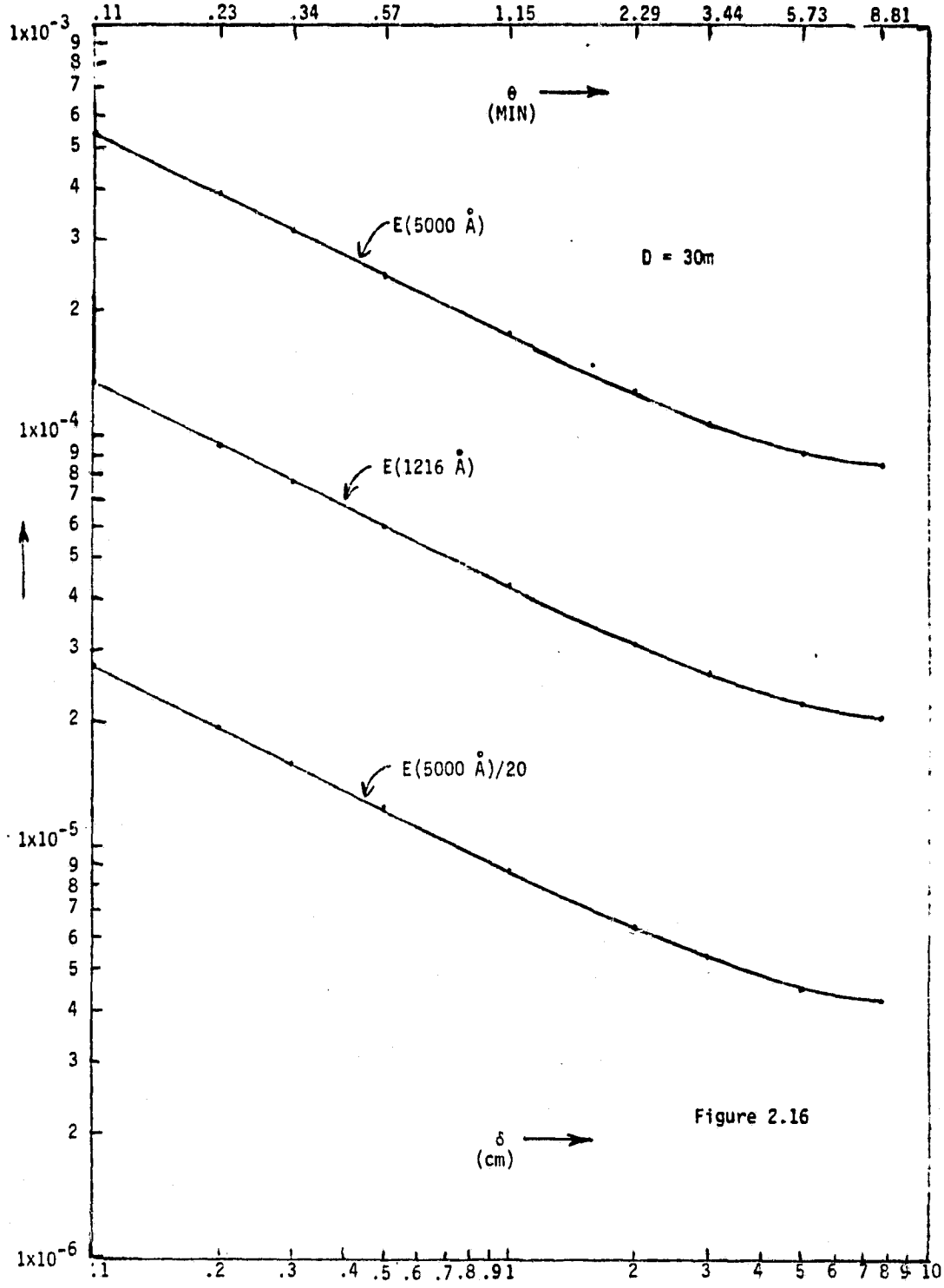
.11
.23
.34
.57
1.15
2.29
3.44
5.73
8.81
θ
(MIN)
E(5000 Å)
D = 30m
E(1216 Å)
E(5000 Å)/20
δ
(cm)
1x10-3
1x10-4
1x10-5
1x10-6
.1
.2
.3
.4
.5
.6
.7
.8
.9
1
2
3
4
5
6
7
8
9
10

Figure 2.16

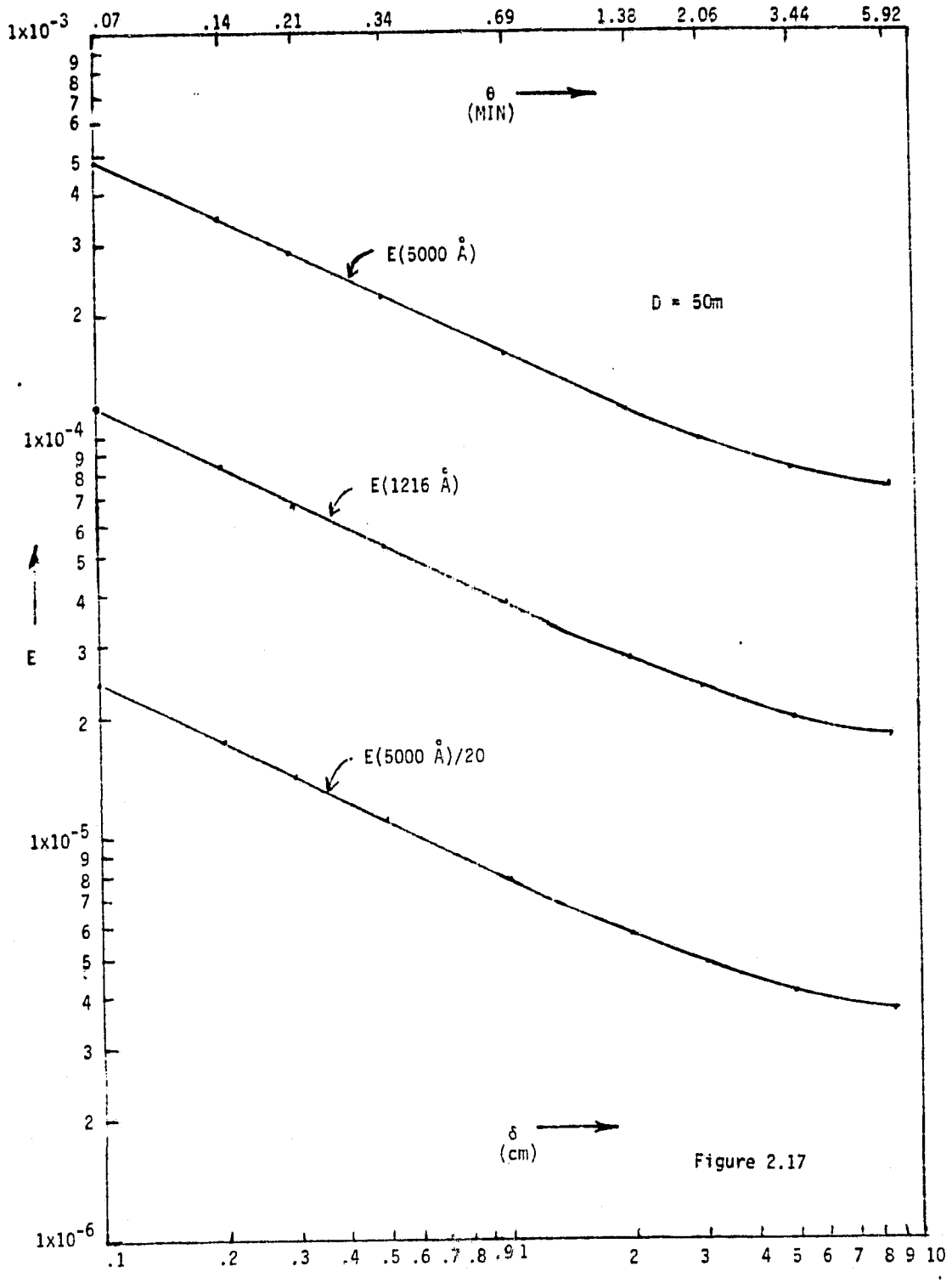

Figure 2.17

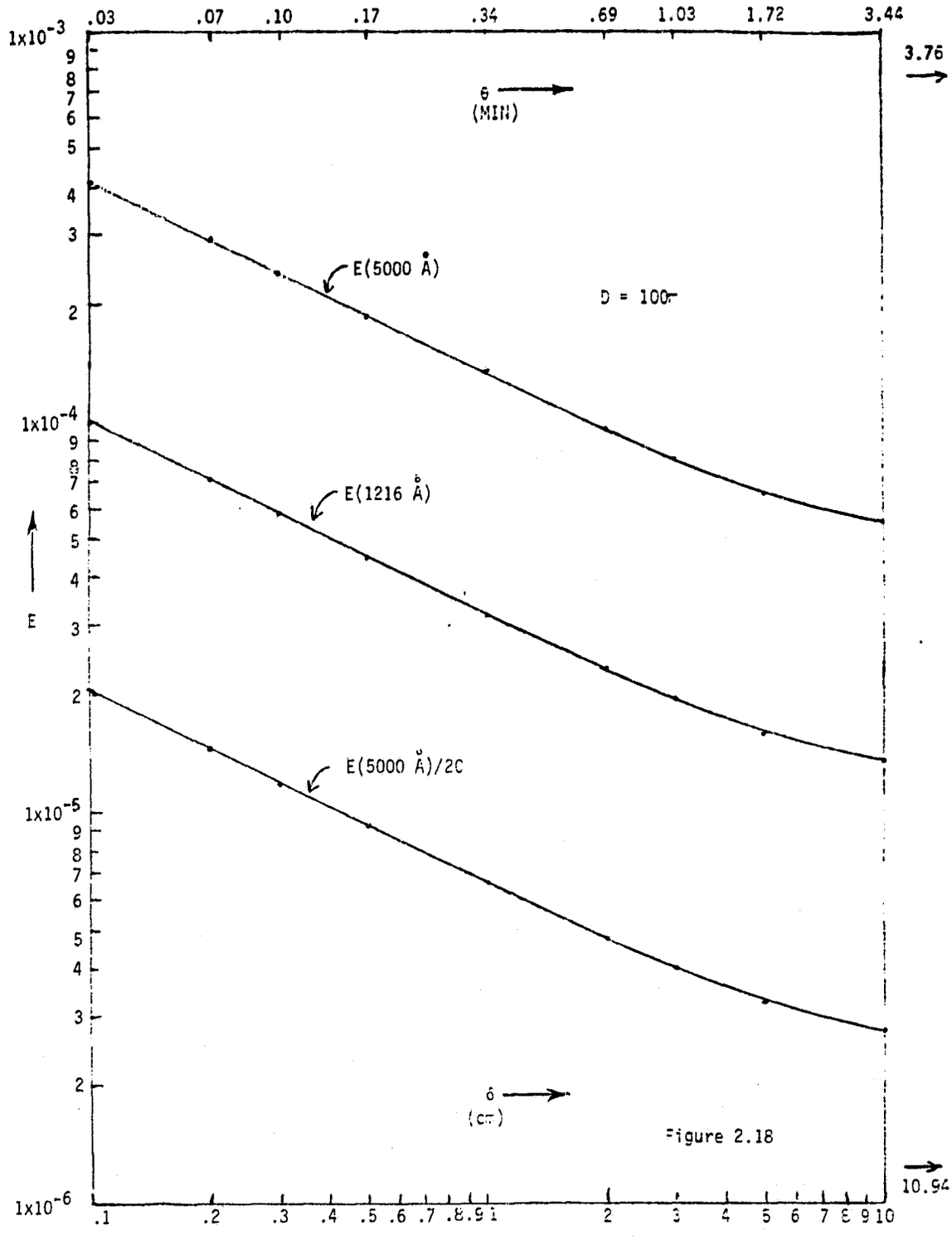
.03
.07
.10
.17
.34
.69
1.03
1.72
3.44
3.76
θ
(MIN)
1x10-3
E(5000 Å)
D = 100
1x10-4
E(1216 Å)
E
E(5000 Å)/2C
1x10-5
δ
(cm)
10.94
1x10-6
.1
.2
.3
.4
.5
.6
.7
.8
.9
1
2
3
4
5
6
7
8
9
10

Figure 2.18

3.0 Stray Light Calculations

In this section, calculations are made of the expected stray light levels in the White Light and UV coronagraphs due to solar radiation scattered along various paths involving the earth, the Shuttle, and the rear surface of the occulter. Two general cases are considered: the backlighted case, in which radiation from the fully illuminated earth falls on the rear surface of the occulter; and the sidelighted case, in which the spacecraft is directly above the earth's terminator. These two cases can be considered to be at, or near, opposite extremes of the possible illumination geometries, with the other cases lying in between. In these calculations, a 200 nautical mile orbit is assumed.

Figure 3.1 illustrates a number of possible techniques for suppressing the stray light illuminating the back of the occulter. In Figure 3.1a, the back of the occulter has simply been given a nonreflective surface, such as a diffuse black coating. In 3.1b, the portion of the occulter directly above the coronagraph has been formed into a concave spherical black mirror whose center of curvature coincides with the coronagraph entrance aperture. (A "black mirror" is a mirror formed from a black glass, acrylic, or other dark material which can be polished. The broadband reflectance of a black mirror will be 4 or 5%, which is somewhat higher than that of most flat black coatings. However, the reflections from a black mirror will mainly be specular, and thus the stray reflected light can be usually sent in some direction in which its effect is harmless.) As shown in Figure 3.1b, rays from the spherical black mirror which are sent toward the coronagraph aperture must have originated in or near that aperture. However, the radiance of the region in or near the entrance aperture can be kept low. Light from the direction of the sunlit shuttle or earth will either be absorbed or specularly reflected in a harmless direction, as indicated. Figures 3.1c and 3.1d show other techniques using black mirrors which are appropriate for the back lighting and side lighting geometries, respectively. Finally, in Figure 3.1e, the back face of the occulter is covered with small black specular dihedrals, cube corners, or pyramids. Stray light is attenuated by multiple reflections from the black faces of these structures. Again, the residue can be sent in some controlled and harmless direction since the reflections are predominently specular.

STRAY LIGHT SUPPRESSION TECHNIQUES

(A)

NONREFLECTIVE
COATINGS

CORONAGRAPH

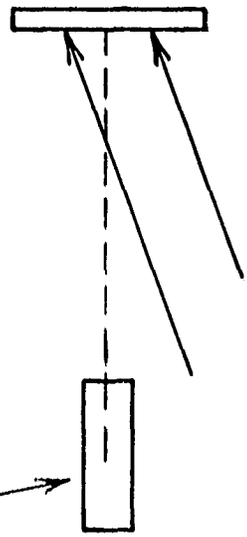

(B)

SPHERICAL
BLACK
MIRROR
(BACK LIGHTING)

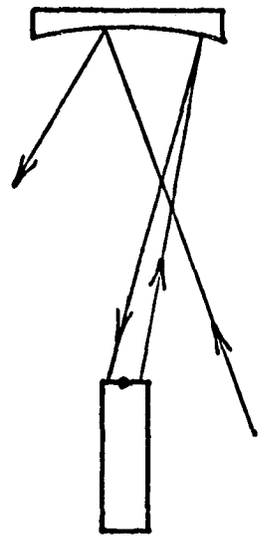

(C)

CONICAL
BLACK
MIRROR
(BACK LIGHTING)

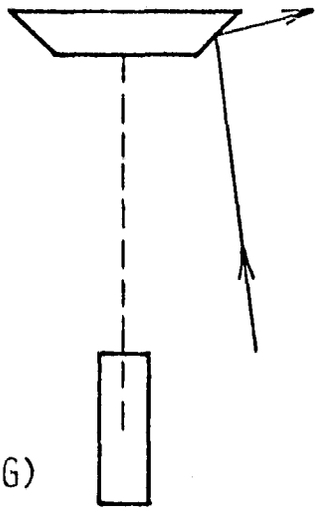

(D)

PLANAR
BLACK
MIRROR
(SIDE LIGHTING)

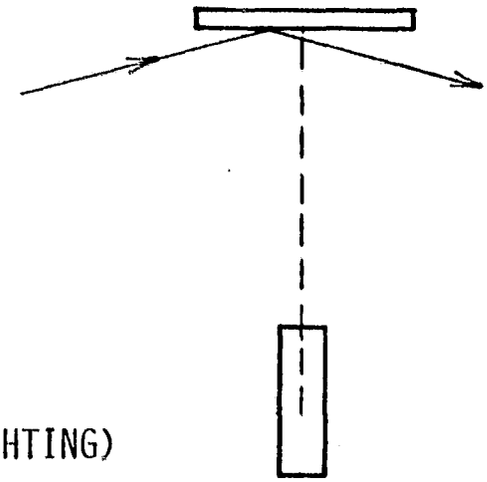

BLACK
SPECULAR
DIHEDRALS,
CORNER
CUBES,
OR PYRAMIDS

(E)

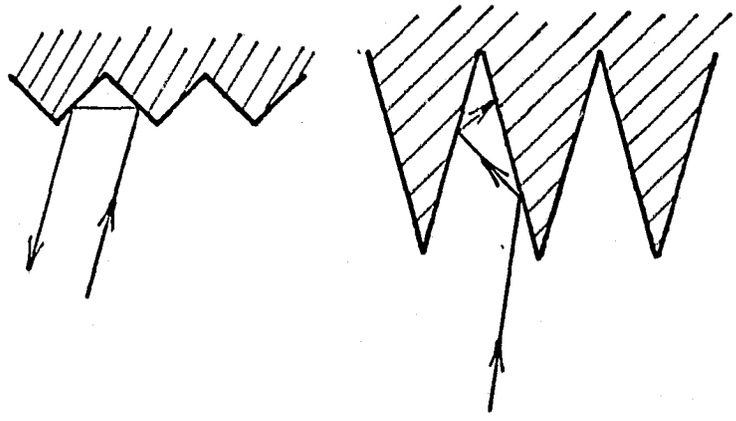

Figure 3.1

3.1 Backlighted Case: White Light

Figure 3.2 shows the principal stray light paths into the entrance aperture of the White Light Coronagraph for the backlighted case (in which the earth and sun lines are approximately 180° apart, as seen from the Shuttle). In Path A, sunlight reflected from the earth illuminates the back of the occulter, and then passes into the coronagraph optical system. In Path B, sunlight reflected from the earth scatters off of the boom, and then into the optics. In Path C, the sunlight reflects from surfaces of the Shuttle, and then adds to the illumination of the back side of the occulter.

In the backlighted case, the stray light calculations for Paths A and C can conveniently be combined. This is because, as viewed from the back of the occulter, the outline of the Shuttle will fall within the illuminated disk of the earth, and the reflectances of the earth and the Shuttle can be considered to be comparable (on the order of 0.50). Thus, if the Shuttle were completely removed from view, the additional earth light which had been blocked by the Shuttle will approximately compensate for the illumination previously received from the Shuttle surfaces.

Figure 3.3 illustrates that the Shuttle will in fact fall within the earth's disk for the backlighted case over the full range of possible boom lengths. A line of sight to the horizon makes a 71° angle with the nadir for a 200 nautical mile altitude. As shown in the table, the angle ϕ from the nadir to an extreme of the Shuttle fuselage is always less than this, ranging from 20° for a 50 meter boom to 62° for a 10 meter boom. (The tip of the vertical stabilizer will protrude beyond the angle ϕ. However, it will mainly be viewed edge-on, and its additional contribution to the illumination of the occulter will be small).

Assuming that the Astromast boom can be made dull black in some way, the stray light calculations for Paths A and B can similarly be combined. This is because, as viewed from the cornonagraph entrance pupil, the outline of the Astromast will fall mainly within the perimeter of the occulter. In communications with Astromast, Inc., actual blackening of the boom surfaces was not recommended. Instead, the recommended technique was deploying the mast within a dull black plastic sleeve made of .0005 in. Mylar or Kapton. This has been done with boom-mounted magnetometers, and Astromast reports that it has been entirely successful.

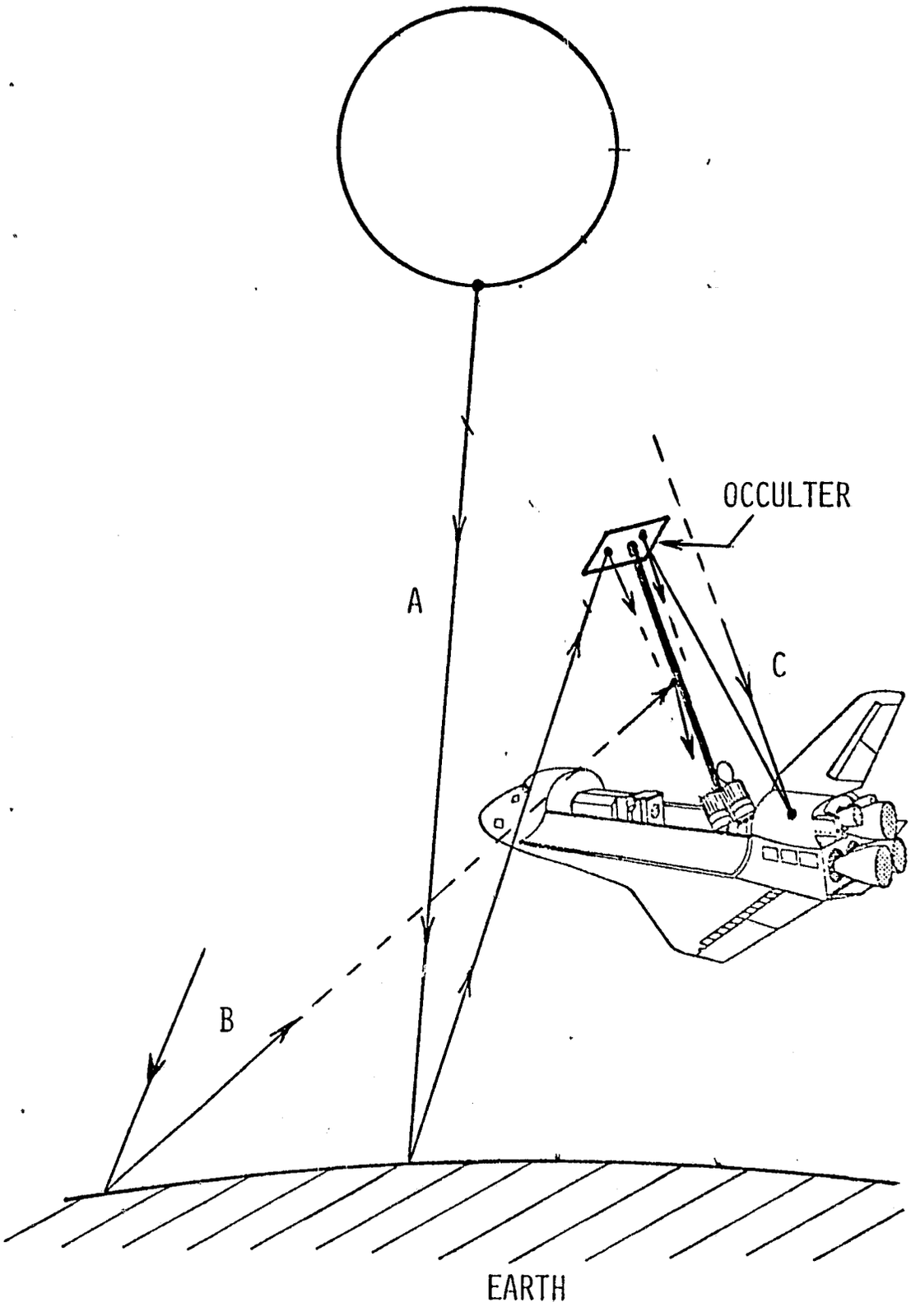

STRAY LIGHT PATHS
(BACK LIGHTED CASE)

Figure 3.2

D	ϕ
10 M	62^0
15 M	51^0
20 M	43^0
30 M	32^0
50 M	20^0

ASSUME 200 NAUTICAL MILE ORBIT

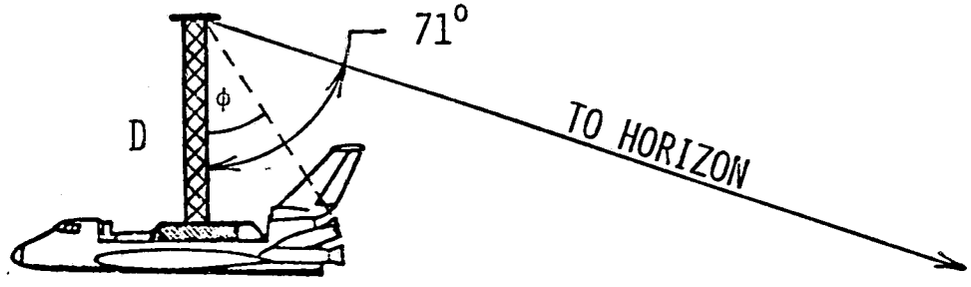

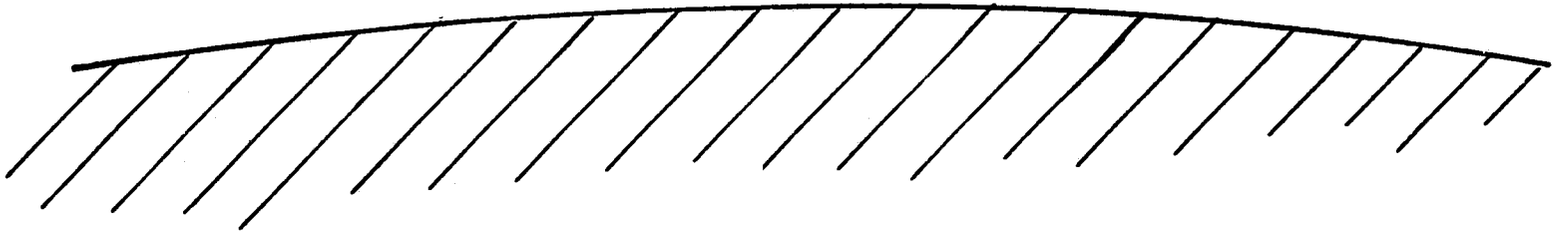

Figure 3.3

Figure 3.4 illustrates the various factors which enter into the backlighting calculation. $I_\odot$ is the radiated flux (not the radiance), in units of power per unit area at the surface of the sun. This flux is reduced at the surface of the earth by the geometrical factor $R_\odot^2/D_E^2$, where $R_\odot$ is the solar radius and D_E is the earth-to-sun distance. The flux which is then reflected back into space is further reduced by a factor A, which is the earth's reflectance or albedo. This flux is then further diminished by a factor F, which is the ratio of the flux at the Shuttle altitude to that which would be observed looking downward from a position just above the earth's surface. Finally, the flux is reduced by the reflectance R of the back side of the occulter. Thus, the flux I_0 scattered from the back surface of the occulter is given by the product of all of these factors:

$$I_0 = \frac{R_\odot^2}{D_E^2} AFRI_\odot \tag{3.1}$$

In order to find the radiance of the back surface of the occulter, let us now assume that the sun is approximately a Lambertian radiator and that the back surface of the occulter is a Lambertian scatterer. (The latter will be approximately correct for most flat black surface coatings). Then, the ratio of the radiances will be equal to the ratio of the fluxes:

$$\frac{B_0}{B_\odot} = \frac{I_0}{I_\odot} \tag{3.2}$$

where B_0 is the radiance of the back of the occulter and $B_\odot$ is the solar radiance. Thus:

$$B_0 = \frac{R_\odot^2}{D_E^2} AFRB_\odot \tag{3.3}$$

Finally, to find the stray radiance B_S in the region of the coronagraph detector plane where the corona will be imaged, we must multiply by a factor H which is a measure of the scattering properties of the coronagraph optics:

$$B_S = HB_0 = \frac{R_\odot^2}{D_E^2} AFRHB_\odot \tag{3.4}$$

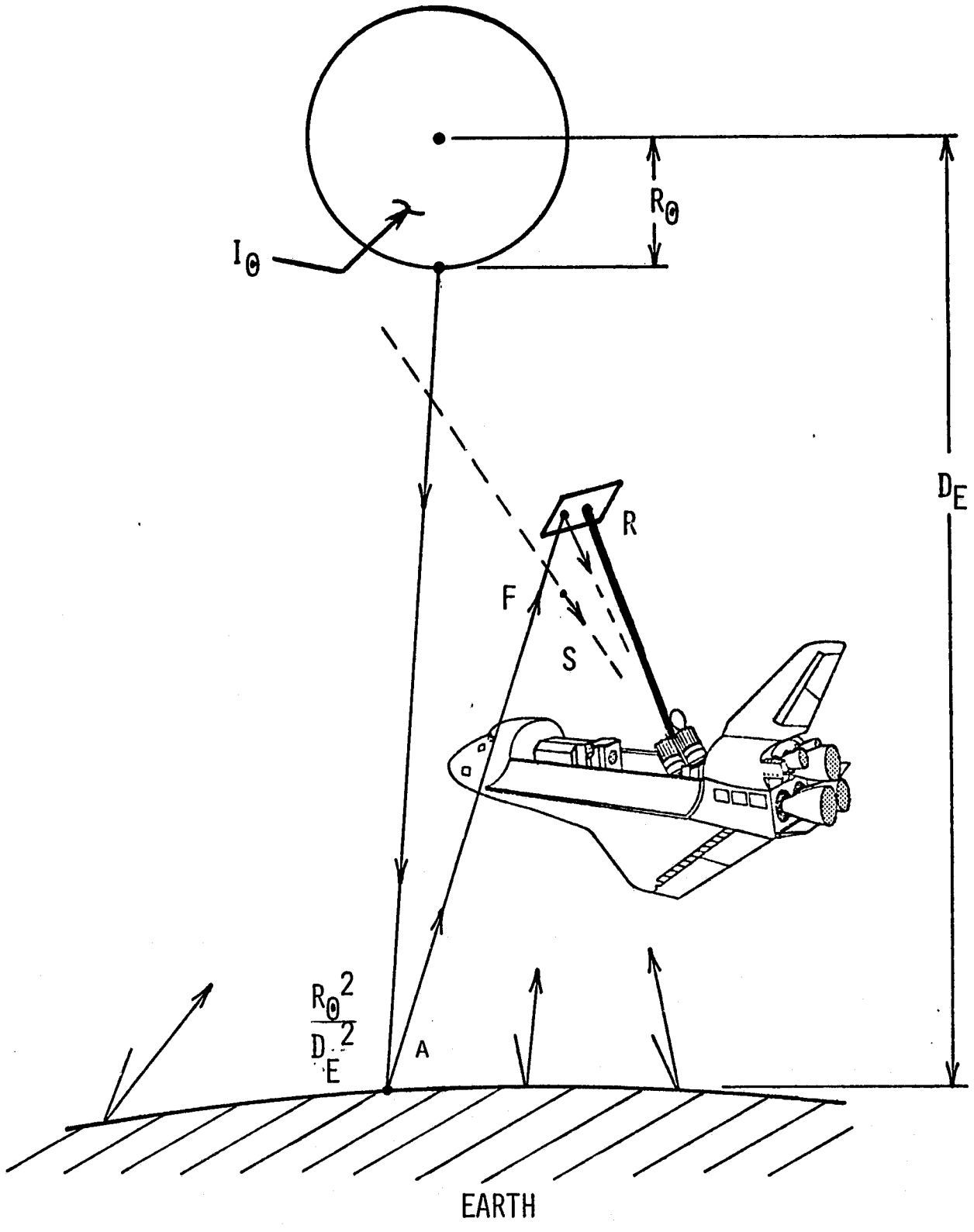

Figure 3.4

Here, H is defined as the stray radiance level observed beyond the edge of the external occulter (due to scattering of light from the occulter by the coronagraph optics) divided by the radiance of the back surface of the external occulter. H would be numerically equal to the conventional coronagraph scattering coefficient H' (where the stray radiance B_S is equal to $H'B_\odot$) if the solid angle of the occulter were equal to the solid angle of the solar disk. The solid angle of the occulter in this case will be larger. However, the contribution to the stray radiance due to regions of the occulter far from the view direction of the coronagraph will be small. The largest contribution will come from regions of the occulter close to the actual occulting edge being used. For this reason, the factor H will be considered to be approximately equal to the conventional coronagraph scattering coefficient H'.

In Table 3.1, numerical values have been assigned to the factors which apply to the backlighted case for the White Light Coronagraph. The value assigned to A of 0.50 is a reasonable estimate of the average diffuse reflectance of the Shuttle and is probably a worst case estimate of the average diffuse reflectance of the earth. The factor F was calculated by numerically integrating over the sunlit face of the earth out to the apparent horizon, assuming the earth to be a Lambertian reflector. This calculation is detailed in Appendix B. Figure 3.5 shows F as a function of the orbital altitude out to 2.0 earth radii. The chosen value of F of 0.88 corresponds to the nominal 200 nautical mile orbit. Finally, the value for the occulter reflectance R of 0.05 was considered to be representative of various non-reflective coatings such as those listed in Table 3.2. Although some of these coatings have listed reflectances of below 0.02, the actual reflectances in use may be increased due to the effects of dust and surface contamination. Thus, a value of 0.05 is a conservative estimate.

Combining the above factors together using Equation 3.4, we find that $B_S = 2.9 \times 10^{-7}\ HB_\odot$. This relation is used in Figure 3.6 to plot the stray radiance B_S (normalized to the solar radiance $B_\odot$) versus the corresponding scatter coefficient H of the coronagraph optics. Using the acceptable stray radiance criterion of $5 \times 10^{-11}\ B_\odot$, this figure shows that the corresponding required value of H is 2×10^{-4}. However, in modern white light coronagraphs, the value of the scattering coefficient is normally kept well below 1.0×10^{-5}[1,2]. Thus, it is concluded that, for the backlighted case in the visible range, the stray radiance due to illumination of the back surface of the

[2] G. NewKirk and D. Bohlin, Appl. Opt. 2, 131 (1963)

TABLE 3.1

NUMERICAL VALUES, BACKLIGHTED CASE

$$\frac{R_{\odot}^2}{D_E^2} = 2.2 \times 10^{-5}$$

$A = 0.5$

$F = 0.88$ (FOR 200 NAUTICAL MILE ORBIT)

$R = 0.03$ (TYPICAL FOR NONREFLECTIVE BLACK COATINGS)

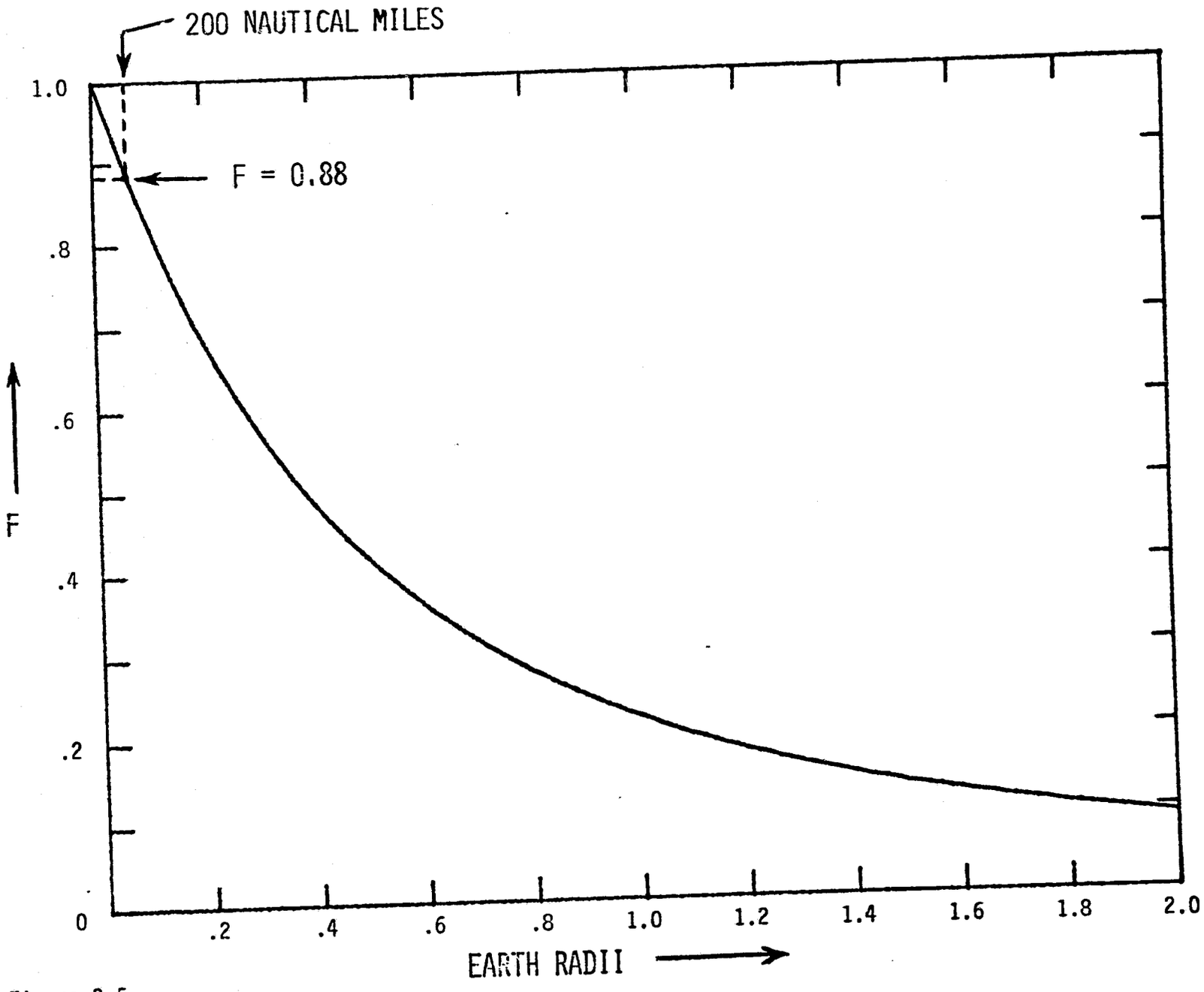
200 NAUTICAL MILES
F = 0.88
1.0
.8
.6
.4
.2
0
F
.2
.4
.6
.8
1.0
1.2
1.4
1.6
1.8
2.0
EARTH RADII

Figure 3.5

TABLE 3.2

NONREFLECTIVE COATINGS

TYPE	REFLECTANCE (λ)	REFERENCE
EVAPORATED GOLD BLACK	1.2% (5460Å)	EPPLEY LABORATORY BULLENTIN NO. 3, MARCH 1971
SINTERED GLASS CONTAINING BLACK LEAD	1.8% (RED)	G. LEWIN, APPL. OPT. 4, 1203 (1965)
PARSONS OPTICAL-BLACK LACQUER	1.3% (5460Å)	HANDBOOK OF OPTICS, McGRAW HILL, P. 7-140 (1978)
3M #401-C10 NEXTEL	2.8% (4000-6500Å)	LEINERT AND KLÜPPELBERG, APPL. OPT. 13, 556 (1974)
HUGHSON CHEMICAL CORP. CHEMGLAZE	3.6% (4000-6500Å)	LEINERT AND KLÜPPELBERG, APPL. OPT. 13, 556 (1974)

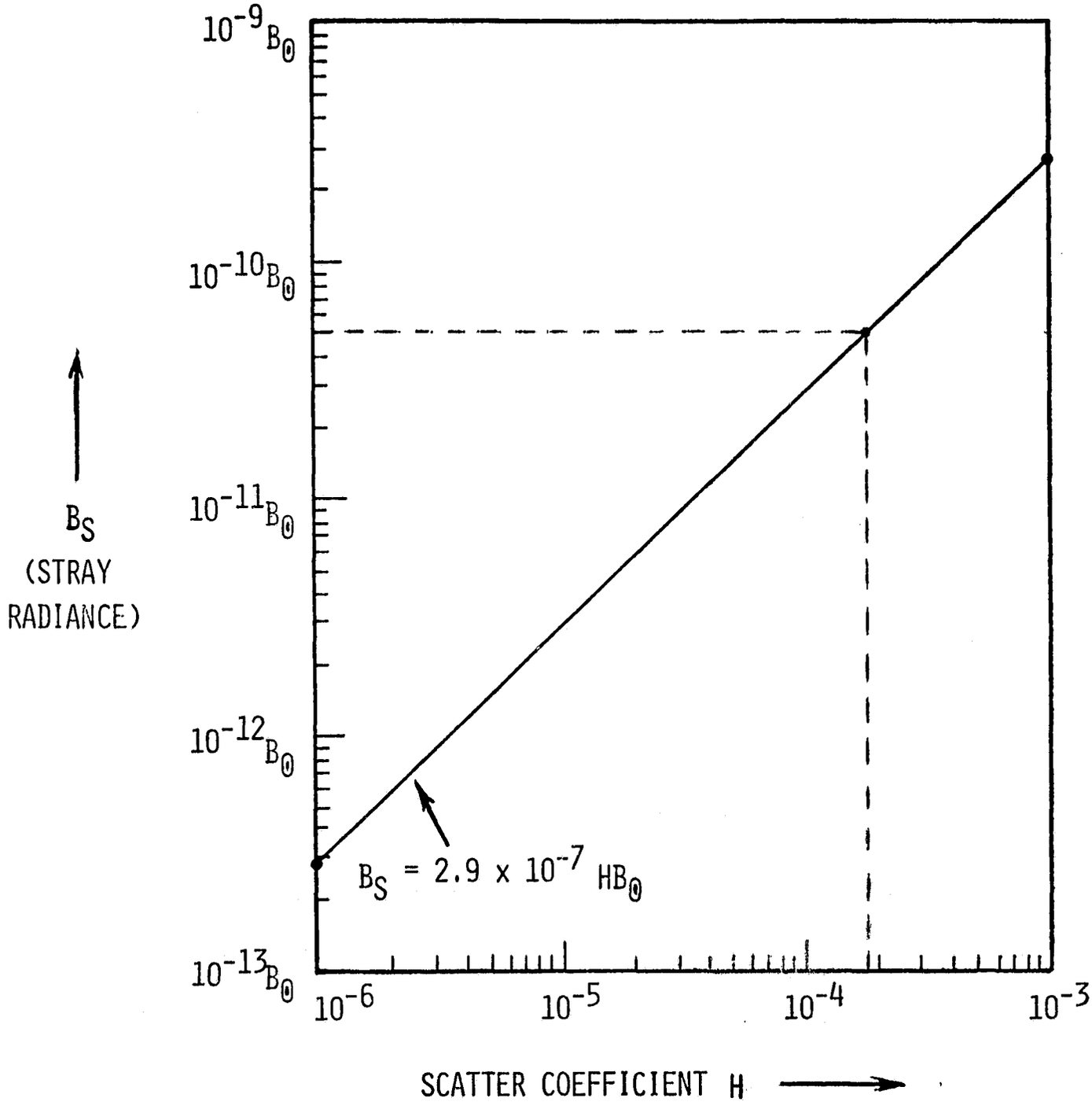
$10^{-9}B_0$
$10^{-10}B_0$
$10^{-11}B_0$
$10^{-12}B_0$
$10^{-13}B_0$
B_S
(STRAY
RADIANCE)
$B_S = 2.9 \times 10^{-7} HB_0$
10^{-6}
10^{-5}
10^{-4}
10^{-3}
SCATTER COEFFICIENT H

Figure 3.6

occulter will present no problem provided that this surface has a diffuse reflectance on the order of 0.03 or less.

3.2 Sidelighted Case: White Light

In the sidelighted case, in which the spacecraft is located directly above the earth's terminator, the Shuttle will no longer appear to fall within the illuminated region of the earth as viewed from the occulter. Thus, the stray light contributions from the Shuttle and the earth must be considered separately.

The major differences between the backlighted and sidelighted cases for the earth's contribution involve the factor F and the grazing angle of incidence of the earthlight on the back surface of the occulter. The latter decreases the apparent crossection of the occulter with regard to the incident light. A third possible difference is that, for many diffuse surface coatings, there is a specularly reflected component for light which is incident at low angles, which would tend to reduce the amount of light diffusely reflected normal to the surface (toward the entrance pupils of the instruments)

The factor F for the sidelighted case is plotted in Figure 3.7. (The ordinate scale here has been changed from that of Figure 3.5). F is equal to zero at zero altitude because, directly on the terminator, the illumination in the model which was used for this calculation is incident at a grazing angle of zero, and thus the surface irradiance is zero. At the nominal orbital altitude of 200 nautical miles, the value of F is 0.018, which is about 50 times smaller than the corresponding value for the backlighted case.

Because the value of F at 200 nautical miles is so much smaller here, the major contribution to the stray irradiance of the occulter will probably come from the Shuttle. Thus, it would be useful at this point to go on to that calculation.

The major difference between the backlighted case and the sidelighted case involving the Shuttle alone once again involves the Factor F. Previous calculations of F assumed that the reflector (the earth) was Lambertian. Because of the complex shape of the Shuttle, the Lambertian effects will be neglected now to simplify the calculation, and F will simply be assumed to be

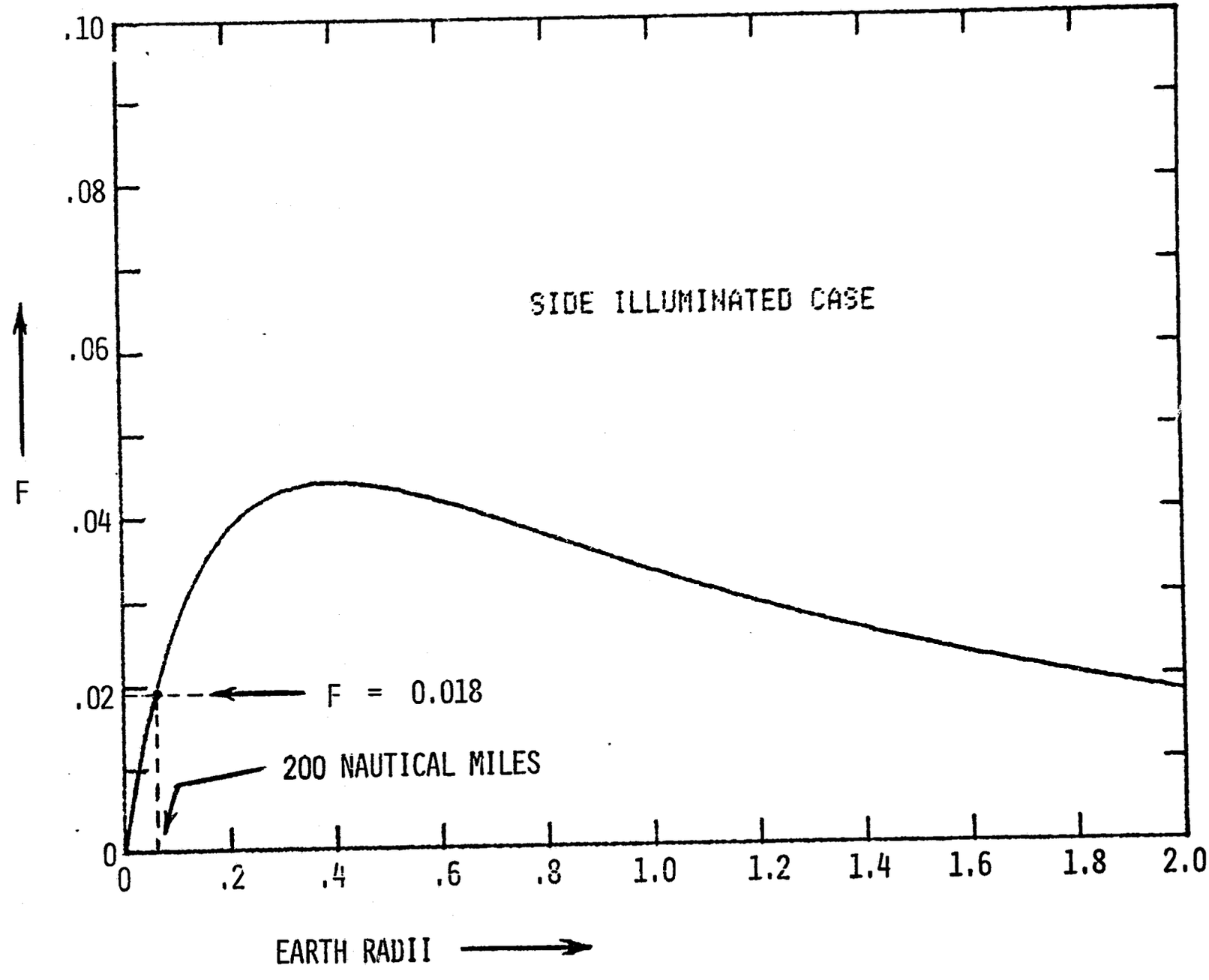
.10
.08
.06
.04
.02
0
F
SIDE ILLUMINATED CASE
F = 0.018
200 NAUTICAL MILES
0
.2
.4
.6
.8
1.0
1.2
1.4
1.6
1.8
2.0
EARTH RADII

Figure 3.7

proportional to the solid angle of the Shuttle as seen from the occulter. The new form F' for the factor F is equal to $\Omega/2\pi$, where Ω is the solid angle subtended by the Shuttle. The factor $1/2\pi$ is used here because F, as defined in the backlighted case, was equal to 1.00 when the solid angle of the earth was 2π. Then, let the solid angle of the Shuttle be approximately equal to C/D^2, where C is the crossectional area of the Shuttle as seen from above, and D is the boom length. Then, F' is given by:

$$F' \approx C/2\pi D^2 \qquad (3.5)$$

(This expression disregards some geometrical factors which would tend to reduce F' for the shorter boom lengths, but should be correct within a factor of 2). Assuming a value for C of 3700 ft^2 or 345 m^2 with the cargo bay doors open, values of F' for various boom lengths D are tabulated below:

TABLE 3.3

D	F'
10 m	.55
20 m	.14
30 m	.061
40 m	.034
50 m	.022

Comparing these values of F' to the 0.018 value of F for the sidelighted earth contribution, it is clear that the earthlight can be neglected for all but the longest boom lengths, where the contributions of the earth and the Shuttle become comparable. Also, comparing the tabulated values of F' to the value of F of 0.88 for the backlighted case (and leaving the other factors $R_\oplus^2/D_E^2$, A, R, and H the same), it is evident that the backlighted case is the worst case, and that the stray light levels will be lower in the sidelighted geometry.

3.3 Stray Light Levels: Ultraviolet

In the vacuum ultraviolet, the reflectances or albedos of the earth and the Shuttle are not likely to be comparable, as they are in the visible region. Therefore, the stray light level calculations should not be combined, as they were in Section 3.1.

In calculating the stray radiance level due to the earth alone in the vacuum ultraviolet, the reflectance of the atmosphere of the earth is not the sole contributer, since a portion of the observed radiance is due to airglow. However, measurements of the earth's radiance in the VUV due to all phenomena including airglow are available, and can be used as a starting point in the stray radiance calculation. Figure 3.8 shows measurements of the atmospheric radiance made by Huffman, et al,[3] with a photometer which was flown on the SAMSO Space Test Program satellite S3-4 in 1978. These measurements were made through a filter nominally centered at 1216 Å, with a full width at half maximum of 116 Å. The peak radiance observed above the midday earth is seen to be 1×10^7 photons/cm^2 sec sr Å. Since the passband of the filter is known to be approximately Gaussian in profile (from private communications), and since the area of a Gaussian of unity height with a FWHM of 116 units is 123, then the total earth radiance B_E observed through this filter was 1.2×10^9 photons/cm^2 sec sr. Emitting features contributing to this radiance level are the Lyman alpha line at 1216 Å and the oxygen resonance lines at 1304 Å and 1356 Å. However, since the oxygen lines are considerably weaker than the Lyman alpha and since they are located far from the center of the filter passband, the predominate part of the observed radiance can be considered to be Lyman alpha.

It is clear from the results of the previous calculations in white light that the stray radiance levels from the earth are higher with backlighting than with sidelighting, so only the backlighted case will be considered here. Let I_E be the radiated flux (power per unit area) from the earth's atmosphere. Assuming that this flux is radiated in a Lambertian

[3] R. Huffman, F. LeBlanc, J. Larrabee, and D. Paulsen, "Satellite Atmospheric Radiance Measurements in the Vacuum Ultraviolet", Air Force Geophysics Laboratory Report AFGL-TR-79-0151, 5 July 1979

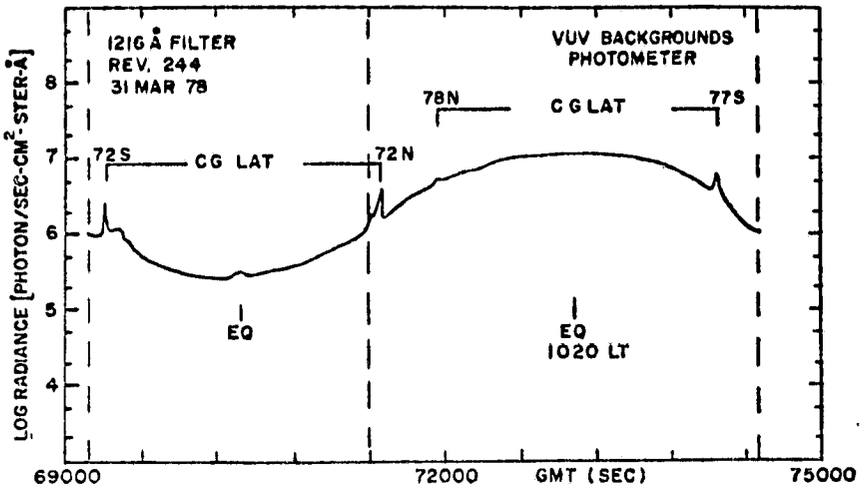

Figure 3.8. Photometer Global Survey (1216 Å Filter)

(From: R. Huffman, F. LeBlanc, J. Larrabee, and D. Paulsen, "Satellite Atmospheric Radiance Measurements in the Vacuum Ultraviolet", Air Force Geophysics Laboratory Report AFGL-TR-79-0151, 5 July 1979).

pattern, the flux at the nominal 200 nautical mile orbit will be diminished by a factor F of 0.88, as before. Then, the flux I_0 scattered from the back surface of the occulter will be:

$$I_0 = FRI_E \tag{3.6}$$

where R is the reflectance of the occulter. Again, assuming that the back surface of the occulter is a Lambertian scatterer, the radiances will be proportional to the fluxes, as in Equation 3.2. Thus, Equation 3.6 can be rewritten as:

$$B_0 = FRB_E \tag{3.7}$$

where B_0 and B_E are the radiances of the back surface of the occulter and of the earth, respectively. Finally, the stray radiance B_S in the UV coronagraph detector plane can be found by multiplying by a coronagraph scattering coefficient H:

$$B_S = HB_0 = FRHB_E. \tag{3.8}$$

As before, H is defined as the stray radiance level observed beyond the edge of the external occulter (due to scattering of light from the occulter by the coronagraph optics) divided by the radiance of the back surface of the occulter. The main contribution to this scattering coefficient will come from the primary mirror of the coronagraph.

The Lyman alpha radiance in a dim coronal feature, a coronal streamer at 4 $R_\odot$, has been observed to be 6 x 10^9 photons/cm^2 sec sr [4]. In order to achieve a signal-to-background ratio of 25 in the observation of such

[4] J. Kohl, E. Reeves, and B. Kirkham, "New Instrumentation for Space Astronomy", edited by K. van der Hucht and G. Vaiana, Pergamon Press, New York, 1978

a feature, the stray radiance B_S would have to be reduced to 2.4×10^8 photons/cm^2 sec sr. Using previous value for B_E of 1.2×10^9 photons/cm^2 sec sr for the earth radiance in Lyman alpha and a value of .88 for F, then from Equation 3.8 the product RH must be equal to or less than .23 to make this observation. Strictly speaking, this result is only valid if the widths of the Lyman alpha lines from the coronal emission and from the earth's atmosphere are equal (that is, if they are spread out over equal areas in the spectrometer image plane). However, in practice, the product RH is likely to be several orders of magnitude smaller than .23, so there is plenty of margin for error. Consequently, no problems are anticipated in the Lyman alpha due to backlighting of the occulter by stray radiance from the earth.

The stray radiance level due to backlighting of the occulter by solar VUV radiation scattered from the Shuttle can be calculated from an expression similar to Equation 3.4:

$$B_S = \frac{R_\odot^2}{D_E^2} AF'RHB_\odot \qquad (3.9)$$

Here, approximate values of the solid angle F' of the Shuttle as seen from the occulter for various boom lengths can be found from Table 3.3. The geometrical factor $R_\odot^2/D_E^2$ is 2.2×10^{-5}, as before. The solar flux in the Lyman alpha line above the earth's atmosphere has been observed to be approximately 6 ergs/cm^2 sec [5], which corresponds to a radiance $B_\odot$ of 5.4×10^{15} photons/cm^2 sec sr. Let the acceptable stray radiance level B_S be 2.4×10^8 photons/cm^2 sec sr, as before. Then, from Equation 3.9, the product ARH must be equal to or less than 9.2×10^{-2} for a 50 meter boom or 3.7×10^{-3} for a 10 meter boom in order to make the required coronal streamer observation. VUV reflectance A of the Shuttle does not seem to be available at this time. However, even for values of A approaching 1.00, the product ARH will probably

[5] R. Kreplin, T. Chubb, and H. Friedman, J. Geophys. Research 67, 2231 (1962).

be orders of magnitude below either 9.2×10^{-2} or 3.7×10^{-3}. Thus, no problems are to be expected from backlighting of the occulter due to VUV radiation scattered from the Shuttle.

The effect of one further source of background radiation on the UV Coronagraph should, at some point, be considered: that of the Lyman alpha emission from atomic hydrogen along the direct line of sight from the UV Coronagraph to the corona. Since the altitude of the nominal orbit is only 200 nautical miles, the column density of atomic hydrogen above the spacecraft could be considerable. Also, note that this background radiation arrives along the same optical path as the radiation from the corona, without being scattered or diffracted off of any part of the spacecraft. Thus, unlike other forms of stray radiation, it cannot be controlled or eliminated by stops or baffles or absorbing coatings. Calculation of the effects of the neutral hydrogen emission, and also absorption, are considered to be beyond the scope of the present study.

4.0 Aspect Sensing and Pointing

In this section, aspect sensing and pointing requirements are examined, and some preliminary aspect sensing techniques are developed. The pointing and aspect sensing problem for the Pinhole X-ray/Coronagraph Assembly is somewhat complicated because of the additional degrees of freedom of the occulter as the boom flexes and twists. That is, the usual requirments for pointing and stabilizing the instrument package with respect to the sun are present. However, the motions of the occulter on the end of the long, somewhat flexible boom must be sensed and controlled as well. A particularly unusual requirement here is the need to sense and actively control the roll orientation of the occulter with respect to the instrument package in order to achieve the full spatial resolution capability of the x-ray experiment operating in the Fourier Mode.

The conventional way to sense the pitch and yaw aspect of a solar instrument package is with a sun sensor which detects the position of the solar limb. A sensor of this type which tracks four sectors of the limb, each 90° apart, by looking through a small window in the occulter is described in Sections 4.3 and 4.4. A polarization sensor to detect the roll orientation of the occulter is examined in Section 4.5, and found to lack sufficient sensativity. A system which detects the roll orientation, and the translational position of the occulter as well, is described in Sections 4.6 and 4.7.

4.1 Reference Axes and Pointing Requirements

Figure 4.1 shows the set of reference axes, vectors, and planes which will be used to define the alignment, sensing, and pointing requirements. These references are described as follows:

$\hat{S}$ is the solar vector, pointing from the center of the White Coronagraph entrance aperture toward the center of the solar disk.

$\hat{O}$ is the occulter vector, pointing from the center of the White Light Coronagraph entrance aperture toward a corresponding reference point on the occulter.

$\hat{C}_1$ is a vector which is co-linear with the optical axis of the White Light Coronagraph.

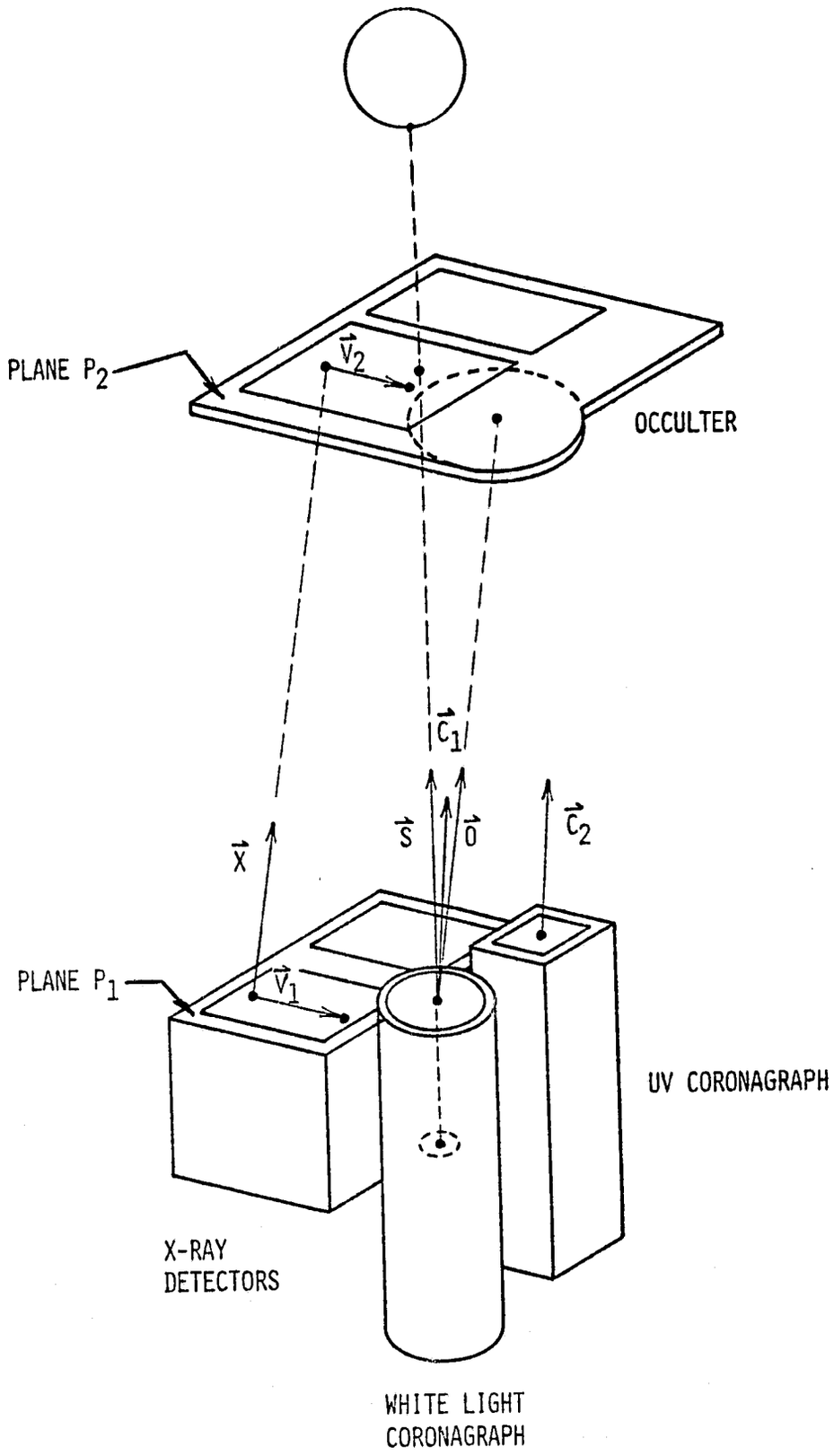
PLANE P_2
$\vec{V}_2$
OCCULTER
$\vec{C}_1$
$\vec{X}$
$\vec{S}$
$\vec{O}$
$\vec{C}_2$
PLANE P_1
$\vec{V}_1$
UV CORONAGRAPH
X-RAY
DETECTORS
WHITE LIGHT
CORONAGRAPH

Figure 4.1

$\vec{C}_2$ is a vector which is co-linear with the optical axis of the UV Coronagraph.

$\vec{X}$ is a vector pointing from a reference point on the near coded aperture toward a corresponding point on the far coded aperture.

P_1 and P_2 are the planes of the near and far coded apertures.

$\vec{V}_1$ is a vector in plane P_1 connecting two reference points on the near coded aperture. $\vec{V}_2$ is a vector in P_2 connecting two corresponding reference points on the far coded aperture.

For the purposes of this study, it is assumed that the internal optical components of the coronagraphs are rigidly aligned with respect to one another and, consequently, that the pointing attitude of each coronagraph can be characterized by a single vector.

Table 4.1 lists a preliminary set of pointing and aspect sensing requirements for the Pinhole X-ray/Coronagraph instruments. Most of the requirements in this table were arrived at by concensus in the course of various meetings and correspondence with members of the Scientific Working Group. The requirements are divided into three categories: absolute pointing and alignment requirements; pointing stability requirements; and aspect sensing requirements. In each case, only the most stringent requirement of each type is listed. Thus, although the x-ray instruments and the UV Coronagraph have absolute pointing requirements with respect to $\vec{S}$ and $\vec{O}$, only the requirements for the White Light Coronagraph are listed since these are judged to be the most stringent.

Under the category of absolute pointing and alignment requirements, the first two requirements ($\vec{C}_1$ parallel to both $\vec{S}$ and $\vec{O}$ to 5 seconds) are derived from the requirement that the White Light Coronagraph be capable of observing the lower corona to within about 0.1 solar radii of the limb. To achieve this, the over-occulting angles of the external and internal occulters can be no more than a couple of arc minutes. Then, in order to reduce the

TABLE 4.1

ABSOLUTE POINTING AND ALIGNMENT REQUIREMENTS

$\vec{C}_1 \parallel \vec{S}$ TO 5 $\widehat{\text{SEC.}}$ (WHITE LIGHT CORONAGRAPH)

$\vec{C}_1 \parallel \vec{O}$ TO 5 $\widehat{\text{SEC.}}$ (WHITE LIGHT CORONAGRAPH)

$\vec{V}_1 \parallel \vec{V}_2$ (IN ROLL) TO 5 $\widehat{\text{SEC.}}$ RMS (X-RAY EXPERIMENT)

$\vec{P}_1 \parallel \vec{P}_2$ TO APPROX. 0.3° (X-RAY EXPERIMENT)

POINTING STABILITY REQUIREMENT

$\vec{C}_1$ STABLE TO $\vec{S}$ WITHIN 0.3 $\widehat{\text{SEC.}}$ OVER 10 SECOND TIME PERIODS (WHITE LIGHT CORONAGRAPH)

ASPECT SENSING REQUIREMENTS

MONITOR MOTION OF $\vec{X}$ WITH RESPECT TO $\vec{S}$ TO .05 $\widehat{\text{SEC.}}$ (X-RAY EXPERIMENT)

MONITOR ORIENTATION OF $\vec{X}$ WITH RESPECT TO $\vec{S}$ TO WITHIN 0.3 $\widehat{\text{SEC.}}$ (0.1 $\widehat{\text{SEC.}}$ IF POSSIBLE)(X-RAY EXPERIMENT).

stray light levels in this coronagraph as far as possible, the images of the sun and the external occulter must be centered on the internal occulting disk to a small fraction of these over-occulting angles. The consensus was that 10 arc seconds could be considered to be this small fraction. Then, the 10 arc second tolerance was equally divided between the first two pointing requirements listed in this table.

The requirements on the roll alignment of $\vec{V}_1$ and $\vec{V}_2$ to 5 seconds RMS and on the parallelism of planes P_1 and P_2 to 0.3° enable the x-ray experiment operating in the Fourier mode to achieve a spatial resolution of about 0.1 seconds. Parallelism of P_1 and P_2 is discussed further in Section 4.2.

The pointing stability requirement ($\vec{C}_1$ stable to $\vec{S}$ within 0.3 arc seconds over a 10 second time period) is derived from the desired angular resolution of 1.0 arc second for the White Light Coronagraph. The 10 second time period is the longest anticipated exposure time for this instrument. The 0.3 arc second smearing due to pointing jitter allows for some further image degradation due to diffraction, aberrations, etc., within the total 1.0 arc second resolution budget.

Under the category of aspect sensing requirements, the relative motion of $\vec{X}$ with respect to $\vec{S}$ must be monitored to 0.05 seconds to compensate for pointing jitter during reconstruction of the x-ray pictures, and thereby allow a spatial resolution of about 0.1 arc seconds to be achieved. Finally, it is necessary to monitor, as a function of time, the absolute orientation of $\vec{X}$ with respect to $\vec{S}$ to 0.3 seconds or better in order to correlate accurately the features in the reconstructed x-ray pictures with corresponding solar features observed with the two coronagraphs and with ground-based instruments.

4.2 Paralleism Requirement on Planes P_1 and P_2

A limit on the allowable amount of boom flexing may be derived from the requirement that the planes P_1 and P_2 of the two coded apertures, operating in the Fourier Mode, remain sufficiently parallel to achieve the desired spatial resolution. In Figure 4.2, lines L_1 and L_2 are parallel lines of sight through corresponding openings at opposite sides of the coded apertures. If the plane of one coded aperture, for instance plane P_2, is tilted through an angle τ, then the line L_2 is shifted through an angle ε to L_2'. The graph in the lower part of the figure shows the dependence of ε on τ for a coded aperture width B of 40 cm and a boom length of 50 meters. In order to reach

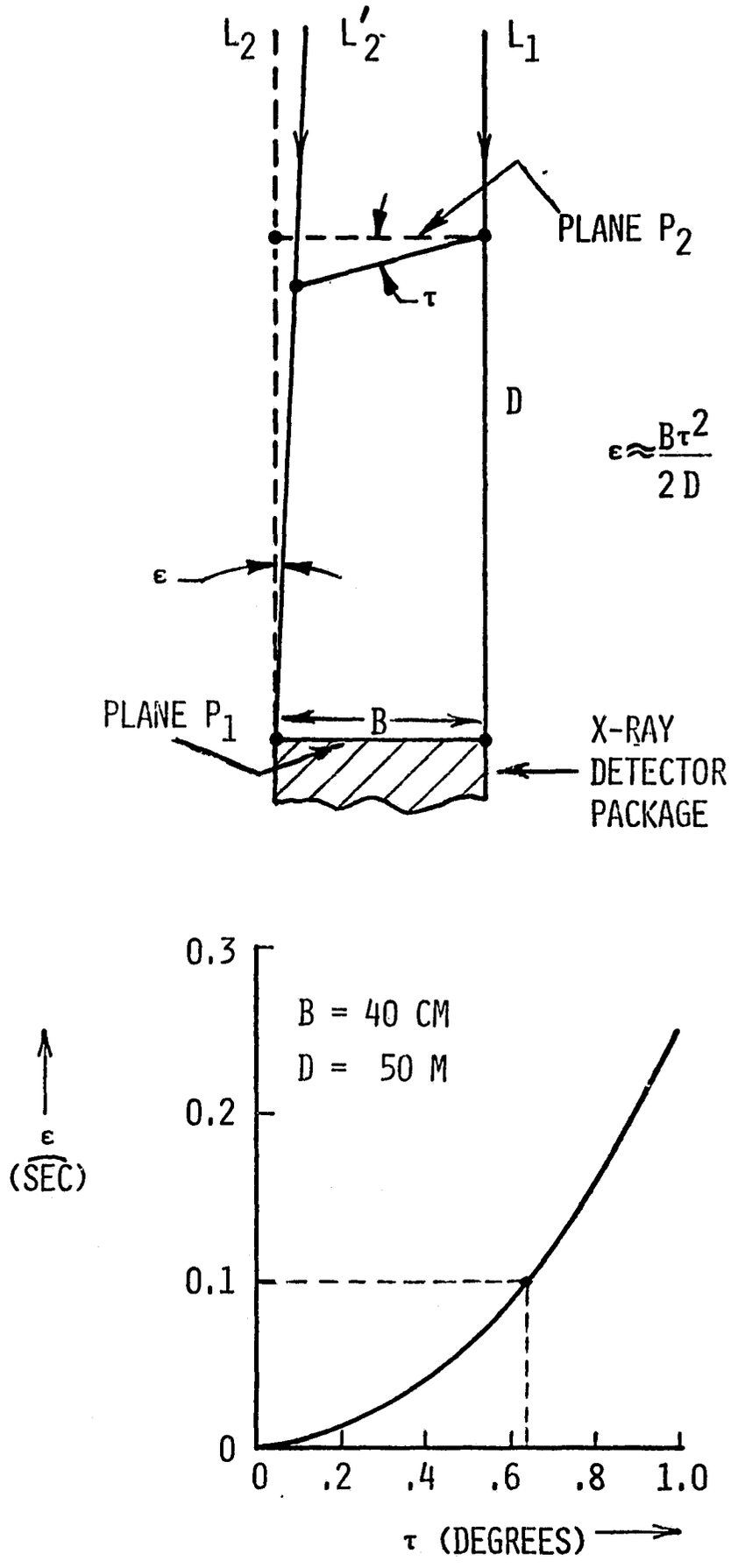
L_2
L'_2
L_1
PLANE P_2
τ
D
$\varepsilon \approx \frac{B\tau^2}{2D}$
ε
PLANE P_1
B
X-RAY
DETECTOR
PACKAGE
0.3
0.2
0.1
0
B = 40 CM
D = 50 M
ε
(SEC)
0
.2
.4
.6
.8
1.0
τ (DEGREES)

Figure 4.2

the desired spatial resolution for this experiment of 0.1 arc seconds, ϵ must be kept somewhat smaller than 0.1 seconds, and thus the non-parallelism τ must be kept somewhat smaller than 0.6 degrees.

4.3 Preliminary Sun Sensor Configuration

The sun sensor must provide error signals to the pointing system in order to satisfy the first of the absolute pointing requirments (alignment of $\hat{C}_1$ t $\hat{S}$) and the pointing stability requirement of $\hat{C}_1$ with respect to $\hat{S}$, to the accuracy listed in Table 4.1. It must also monitor the relative motion (due to pointing jitter) and the absolute orientation of $\hat{C}_1$ with respect to $\hat{S}$, so that, when combined with data from the occulter sensor, the motion and orientation of $\hat{X}$ with respect to $\hat{S}$ can be determined.

An obvious configuration for the sun sensor is one which detects the position of the solar limb in four sectors spaced 90° apart on the edge of the solar disk. The main problem is how to provide the sun sensor with a suitable view of the sun in the presence of the occulter. The final shape of the occulter is not defined at this time, but it may very well be rectangular or an irregular shape, rather than a disk. A sun sensor which views the sun around the edge of the occulter would probably have to be mounted on a protruding arm, which would increase the overall dimensions of the instrument package and perhaps introduce alignment and mechanical stability problems. On the other hand, a window or cutout in the occulter large enough for a conventional sun sensor to view the entire solar disk would probably interfere with the location of the coded apertures, the boom attachment area, or other features on the occulter. A large window might also increase the stray light levels in the coronagraphs.

A configuration which allows the sun sensor to view the sun through a relatively small window in the occulter is shown in Figure 4.3. The required four sectors of the solar limb are viewed through the window by four pentaprisms, each of which relays the view to a corresponding pentaprism located over the sun sensor objective lens. (Only two pairs of the four pairs of pentaprisms are shown in this figure). Pentaprisms are used here for their constant deviation characteristic, which simplifies the alignment and mechanical stability requirements. The angular deviation of a ray by a pentaprism in a plane mutually perpendicular to entrance and exit faces of the prism is a constant, regardless of minor tilts and misalignments of the prism itself.

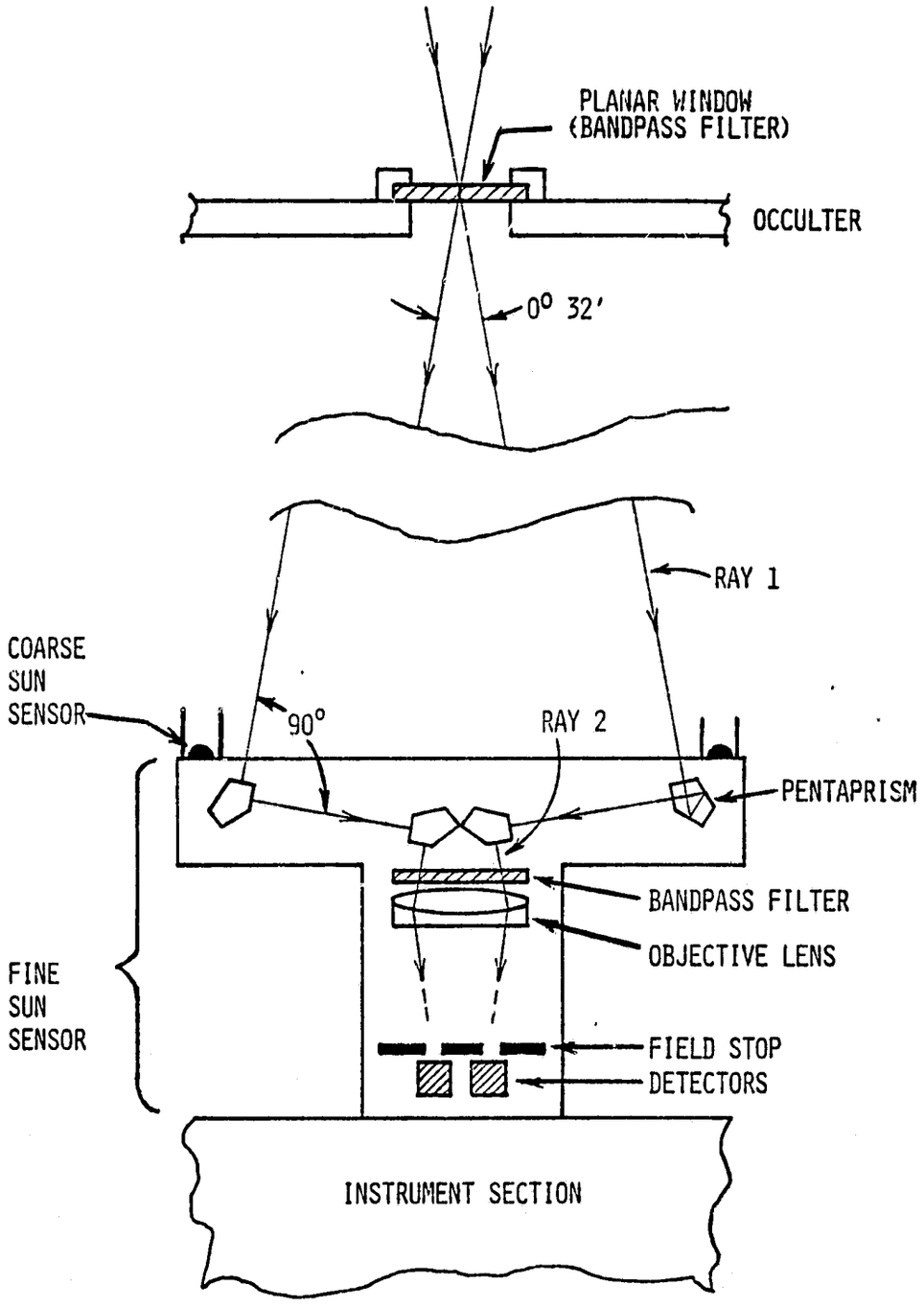
PLANAR WINDOW
(BANDPASS FILTER)
OCCULTER
0° 32'
RAY 1
COARSE
SUN
SENSOR
90°
RAY 2
PENTAPRISM
BANDPASS FILTER
OBJECTIVE LENS
FINE
SUN
SENSOR
FIELD STOP
DETECTORS
INSTRUMENT SECTION

Figure 4.3

Commonly, pentaprisms are made with deviation angles equal to 90°, to within one arc second or better. Thus, in the plane of the diagram (Figure 4.3), Ray 2 will remain parallel to Ray 1 regardless of the angular orientation of either of the pentaprisms involved. Misalignments of the pentaprisms can, however, affect the parallelism of these two rays out of the plane of the diagram. However, this would displace the image of the corresponding sector of the solar limb in a direction tangent to the limb, as indicated by the arrows on the right side of Figure 4.4, and the output of this sun sensor is relatively insensative to image shifts in this direction. Also since the pentaprisms are located before the focussing elements of the sun sensor, in the region where the light from any given object point is collimated, the system is quite insensative to translational motions of the pentaprisms as well. For these reasons, the pentaprisms can probably be positioned and oriented by construction alone.

The spacing between the outer pentaprisms will be approximately equal to the boom length times the angular diameter of the sun. Thus, it would range from about 18.6 cm for a 20 meter boom to about 46.5 cm for a 50 meter boom. Nominal apertures for the window, the pentaprisms, and the objective lens are 5 cm, 2.5 cm, and 8.0 cm, respectively.

The four sectors of the limb are imaged onto the field stop by the objective lens, as shown in Figures 4.3 and 4.4. The field stop contains four cross-shaped cutouts, behind each of which is a separate detector. Nominally, when the sensor is pointed at the center of the sun, the image of the solar limb will lie along the centerline of the arms of each cross which are tangent to the limb, as shown.

The general form of the output signal from a given detector as the image of the limb moves across one of the cross-shaped cutouts is shown in the lower part of Figure 4.4. Initially, the signal rises slowly from zero as the image of the solar disk fills more and more of the inner radial arm of the cross. Then, the slope of the curve suddenly increases as the image begins to fill the tangential arms of the cross, with the signal equal to S_c when the image of the limb lies at an angular position θ_c along the centerline of the cross. Finally, the slope decreases again as the image begins to fill the outer radial arm of the cross. The purpose of the radial arms, of course, is to increase the angular dynamic range of the sensor. The purpose of the tangential arms is to increase the slope of the error signals when the sensor approaches the sun-centered orientation.

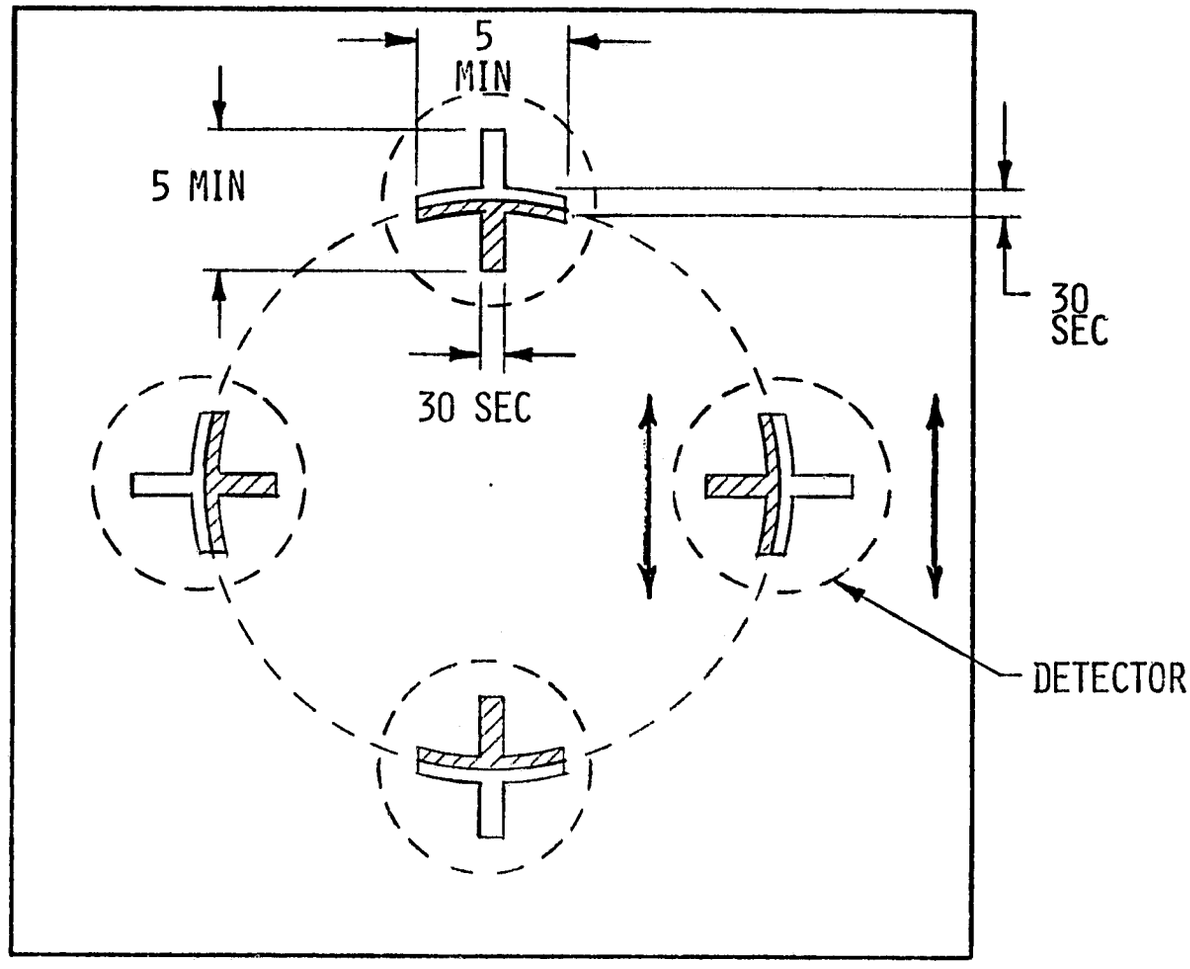

FINE SUN SENSOR FIELD STOP

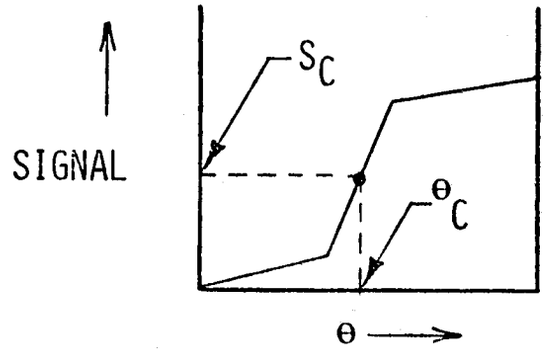

Figure 4.4

Typical dimensions for the crossshaped cutouts are shown in Figure 4.4. The arms are 30 arc seconds wide and a total of 5 arc minutes long, giving a total angular area of 4.75 square minutes for each cross. When nominally centered on the sun, one half the area or 2.38 sq. min. of a cross will be filled with radiation from the solar disk. Then, a change in the angular orientation θ of 5 seconds (the relevant absolute pointing requirement from Table 4.1) corresponds to a change in illuminated area in the cross of .42 sq. min., or to an 18% change in signal level. Similarly, a change in θ of 0.3 seconds (the pointing stability requirement and also the aspect sensing requirement on the absolute orientation, from Table 4.1) results in a signal change of 1.1%. Signal changes of these amounts should be readily detectable, and should also be large compared to the shifts in sensativity of most stable types of detectors which might be used here. Even a change in θ of 0.05 seconds (the aspect sensing requirement on the relative motion) corresponds to a readily detectable signal change of 0.18%, although the detector sensativity may not be stable to this level over long periods of time. However, long term drifts are not important here, because the data on the relative motion will only be used in the reconstruction of individual x-ray exposures, which will be of relatively short duration.

The important point is that, by keeping the tangential arms of the crosses quite narrow (on the order of 30 arc seconds), the resulting fractional changes in signal level with θ which must be detected to satisfy the pointing requirements are relatively large and quite readily detectable. Also, the detrimental effects of long term shifts in detector sensativity levels are minimized when the tangential arms are narrow. This same argument can be used to justify the use of imaging optics in the sun sensor. That is, if the image of the sun on the aperture stop were out of focus by 30 arc seconds or more, the factional change in signal level for a given change θ in orientation would be reduced in proportion to the amount of defocussing.

Returning to Figure 4.3, the purpose of the bandpass filter over the window in the occulter is to prevent radiation passing through the window in the occulter from raising the stray light levels in the White Light Coronagraph. The nominal bandpass of this filter is 8250 Å to 8750 Å. A similar filter is placed over the objective lens of the sun sensor to decrease the effects of stray light on the aspect signals from this sensor by, effectively, "tuning" the sun sensor to the radiation passing through the window in the

occuler. The coarse sun sensors shown in the vicinity of the outer penta-prisms increase the angular dynamic range of the system, and are to be used for initial acquisition of the sun. They are non-imaging photodetectors which use the crude pinhole camera "image" of the sun formed by the occulter window to bring the sun within the 5 arc minute angular range of the imaging sun sensor, which hence forth will be referred to as the Fine Sun Sensor.

4.4 Fine Sun Sensor Electronics and Signal-to-Noise Calculation

A block diagram of the Fine Sun Sensor electronics is shown in Figure 4.5. The signals from opposite pairs of silicon detectors located behind the cross-shaped field stop openings, after passing through integrated preamplifiers, are subtracted in a differiental amplifier, producing an error signal. Gain and bias adjustments on the amplifiers are used for preflight alignment of the vectors $\vec{C}_1$ and $\vec{S}$. Then, in-flight measurments can be made of the stray light levels in the coronagraphs, and further adjustments to the gain and bias levels could be made to correct the fine sun sensor alignment if necessary.

Table 4.2 details a signal-to-noise calculation for the nominal fine sun sensor configuration. The spectral passband is defined by the filters over the occulter window and the objective lens. The illuminated area of tangential part of the cross-shaped cutout is $\Delta\ \theta$ times $\Delta\ \emptyset$. The detector is assumed to be a silicon detector operated in the D.C. (unchopped) mode with a 1.0 second integration time and a noise equivalent power of 10^{-11} watts. Then, if we require a signal-to-noise ratio as large as 1000, the required collecting area is calculated to be only 0.0053 cm^2. This calculation indicates that there should be no signal-to-noise problems with a fine sun sensor of this type.

4.5 Polarization Roll Sensor

Listed in Table 4.1 is a requirement to sense and control the roll orientation of the occulter (or, alternatively, the far coded aperture) to 5 arc seconds RMS. Precise sensing of the angular alignment of two well separated objects in roll is an unusual requirement, and no conventional methods of accomplishing this were uncovered. One possible method which was devised involved the use of crossed polarizers located on the occulter and on the instrument package.

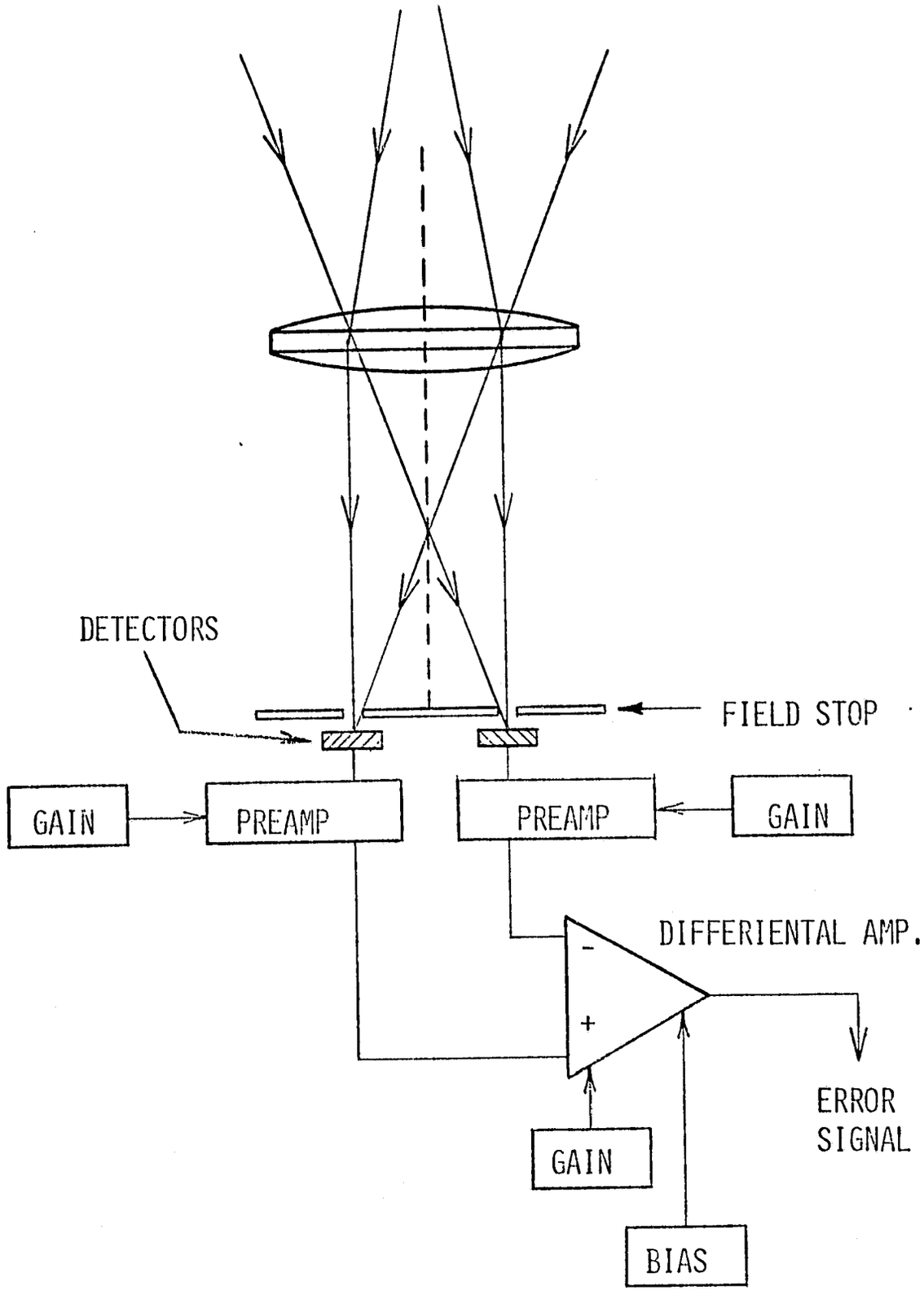
DETECTORS
FIELD STOP
GAIN
PREAMP
PREAMP
GAIN
DIFFERIENTAL AMP.
−
+
ERROR
SIGNAL
GAIN
BIAS

Figure 4.5

TABLE 4.2

SIGNAL-TO-NOISE CALCULATION

PASSBAND: 8250 Å to 8750 Å ($\Delta\lambda$ = .05 μ)

ASSUME THE SUN IS A 5770°K BLACKBODY:

8×10^3 WATTS/CM^2/μm AT λ PEAK

4.6×10^3 WATTS/CM^2/μm AT 8500 Å

1.5×10^3 WATTS/CM^2/μm/SR AT 8500 Å

LET $\Delta\theta$ = 5 ARC MIN AND $\Delta\phi$ = 15 ARC SEC.

$\Omega = 1.0 \times 10^{-7}$ SR.

SILICON DETECTOR (D.C., 1 SEC., 8500 Å)
WITH AN INTEGRATED PREAMP, HAVING A COMBINED N.E.P. OF 10^{-11} WATTS.

TRANSMITTANCE OF FILTERS = .5x.5 = .25

REQUIRE S/N OF 1000:

$$\frac{1.5 \times 10^3 \text{ WATTS/CM}^2\text{/SR/}\mu \times .25 \times .05\ \mu \times 10^{-7} \text{ SR} \times A}{10^{-11} \text{ WATTS}} = 1000$$

THEN:

(REQUIRED COLLECTING AREA) = A = .0053 CM^2

In this scheme, a polarizing prism, such as a Glan-Thompson prism, would be used to linearly polarize a beam of light from a source mounted on the occulter. This polarized beam would then impinge on a second polarizing prism, acting as an analyzer, mounted on the instrument package, and finally pass into a detector. The signal level from the detector would be used to determine the roll error of the occulter relative to the instrument package. (Polarizing prisms would be used here rather than other polarizing materials because prisms generally produce a very clean linearly polarized beam, with a negligible unpolarized residue).

The intensity I of the light transmitted through a pair of polarizers as a function of the roll angle ω between their reference axes is given by:

$$I = I_{max} \cos^2 \omega \qquad (4.1)$$

In order to produce a large fractional change in signal for a small angular change in ω, the polarizers should operate in a crossed or nearly crossed orientation, where ω is approximately equal to 90°. Near 90°, the following approximation can be made:

$$I \approx I_{max} (\omega - \pi/2)^2 \qquad (4.2)$$

This curve is plotted in Figure 4.6.

In order to determine the direction as well as the magnitude of the roll errors, two sets of crossed polarizer sensors would be used. As indicated in Figure 4.6, when the occulter is in the nominal aligned position, one set of prisms would be crossed at ω=89°, and the other set would be crossed at ω=91°. At the ω=90° orientation, the outputs of the two detectors would be equal, and after subtraction in a differiental amplifier, would give an error signal of zero. Then when the occulter rotates in roll, the signal from one detector will increase while the other decreases, giving an error signal whose polarity indicates the direction of the roll error.

The above equation can be used to calculate the signal change ΔI for a given roll error $\Delta\omega$. For a sensor operating at 89° (or 91°), a roll error of 5 seconds will result in a fractional change in signal $\Delta I/I$ of only 2.8×10^{-3}. Since the roll requirement is an absolute alignment requirement, rather

POLARIZATION ROLL SENSOR

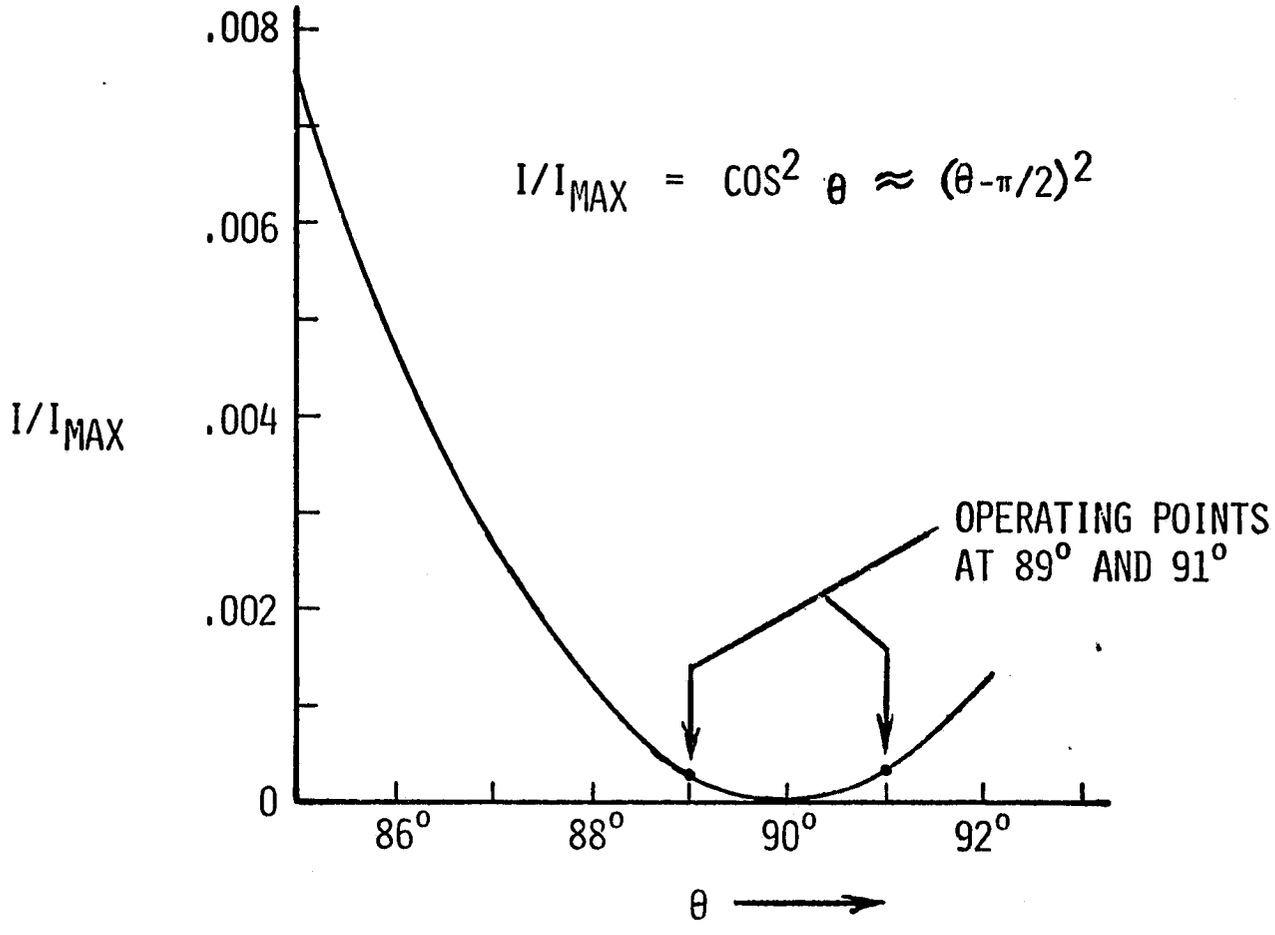

FOR $\Delta\theta$ = 5 SEC:

$\Delta I/I_{MAX} = 8.5 \times 10^{-7}$

$\Delta I/I = 2.8 \times 10^{-3}$

Figure 4.6

than just a stability requirement, the sensativities of the detectors would have to be stable to this level or better, which would be very difficult to achieve in practice. Also, the absolute magnitude of ΔI would be very small, or alternatively the source would have to be very bright, since $\Delta I/I_{max}$ for a 5 second shift is only 8.5×10^{-7}. Shifting the operating points closer to 90° would inprove the $\Delta I/I$ value, but would still involve small signals or bright sources. For this reason, the polarization roll sensor was considered to be too insensative for this application.

4.6 Occulter Sensor Using Tracking Telescopes and Cube Corners

In the course of this study, another occulter sensing technique was considered. This technique has the advantage of providing aspect data on the occulter in pitch and yaw as well as in roll. This system is shown schematically in Figure 4.7. Here, two cube corner retroreflectors mounted as far apart as possible on the occulter are illuminated by two point light sources on the instrument section. It is a property of a cube corner reflector that it will form a virtual image of a point source which is located such that the point source, the vertex of the cube corner, and the virtual image are equally spaced along a straight line, as shown. (A geometrical proof of this is given in Appendix C). The positions of these two virtual images are then sensed by two small telescopes, similar to star trackers except that they are focussed for the range of the virtual images instead of at infinity.

As the occulter moves in pitch and/or yaw, both virtual images will appear to shift in the same direction and by approximately the same angular amount. However, in a roll rotation about, for instance, the geometric center of the occulter, the virtual images will appear to move in opposite directions. Thus, it is possible to distinguish between pitch, yaw, and roll movements.

An advantage of this scheme is that it requires that only passive components (the cube corners) be mounted on the occulter.

More details of the point source and tracking telescope are shown in Figure 4.8. The initial position of the cube corner which is to be illuminated will probably be known to a few tenths of a degree. Thus, the radiant intensity of the point source can be increased with a condenser lens, as shown. The condenser lens effectively relocates the point source to Point P. The tracking telescope then forms an image of the distant virtual image formed

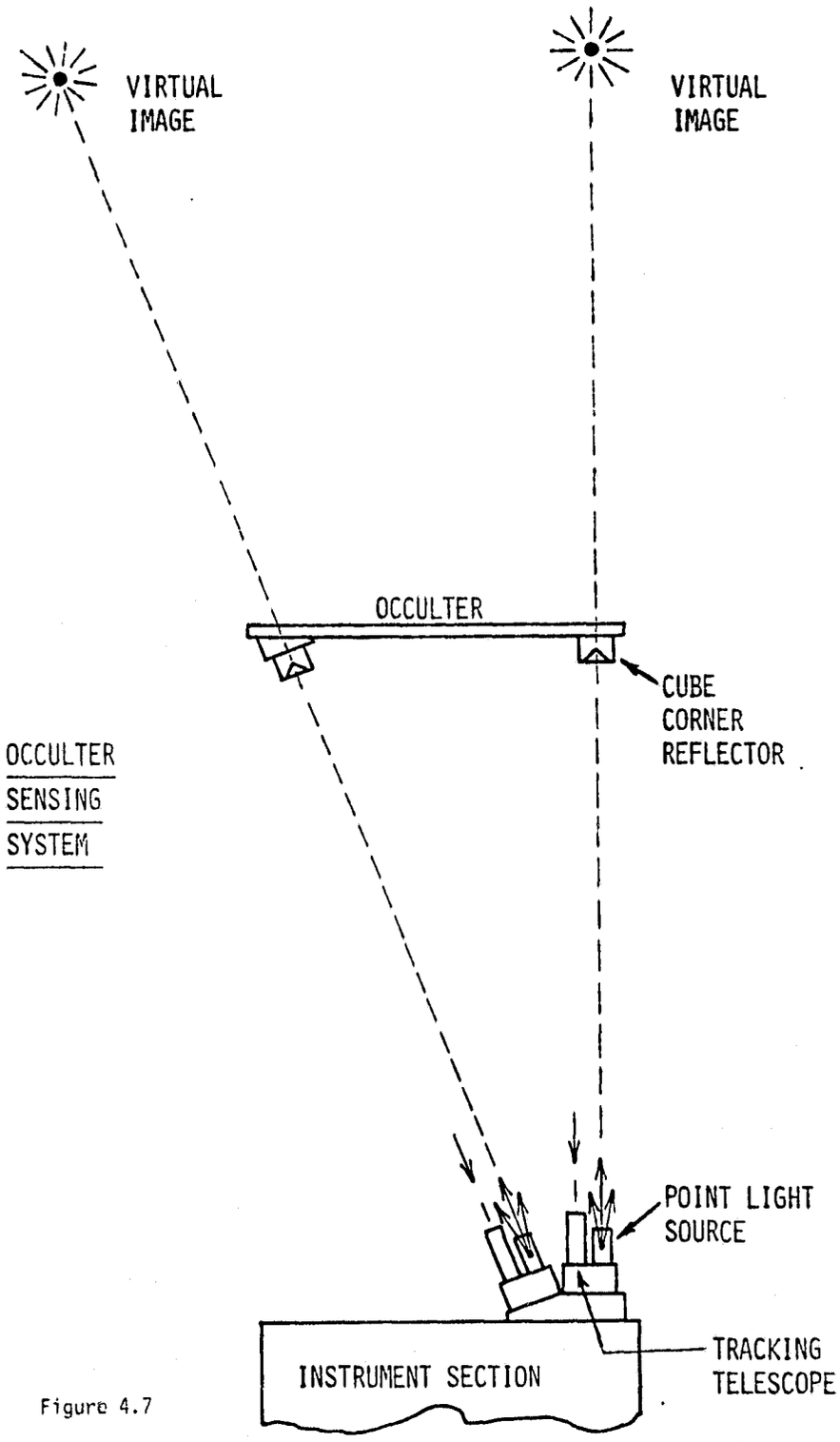
VIRTUAL
IMAGE
VIRTUAL
IMAGE
OCCULTER
CUBE
CORNER
REFLECTOR
OCCULTER
SENSING
SYSTEM
POINT LIGHT
SOURCE
TRACKING
TELESCOPE
INSTRUMENT SECTION

Figure 4.7

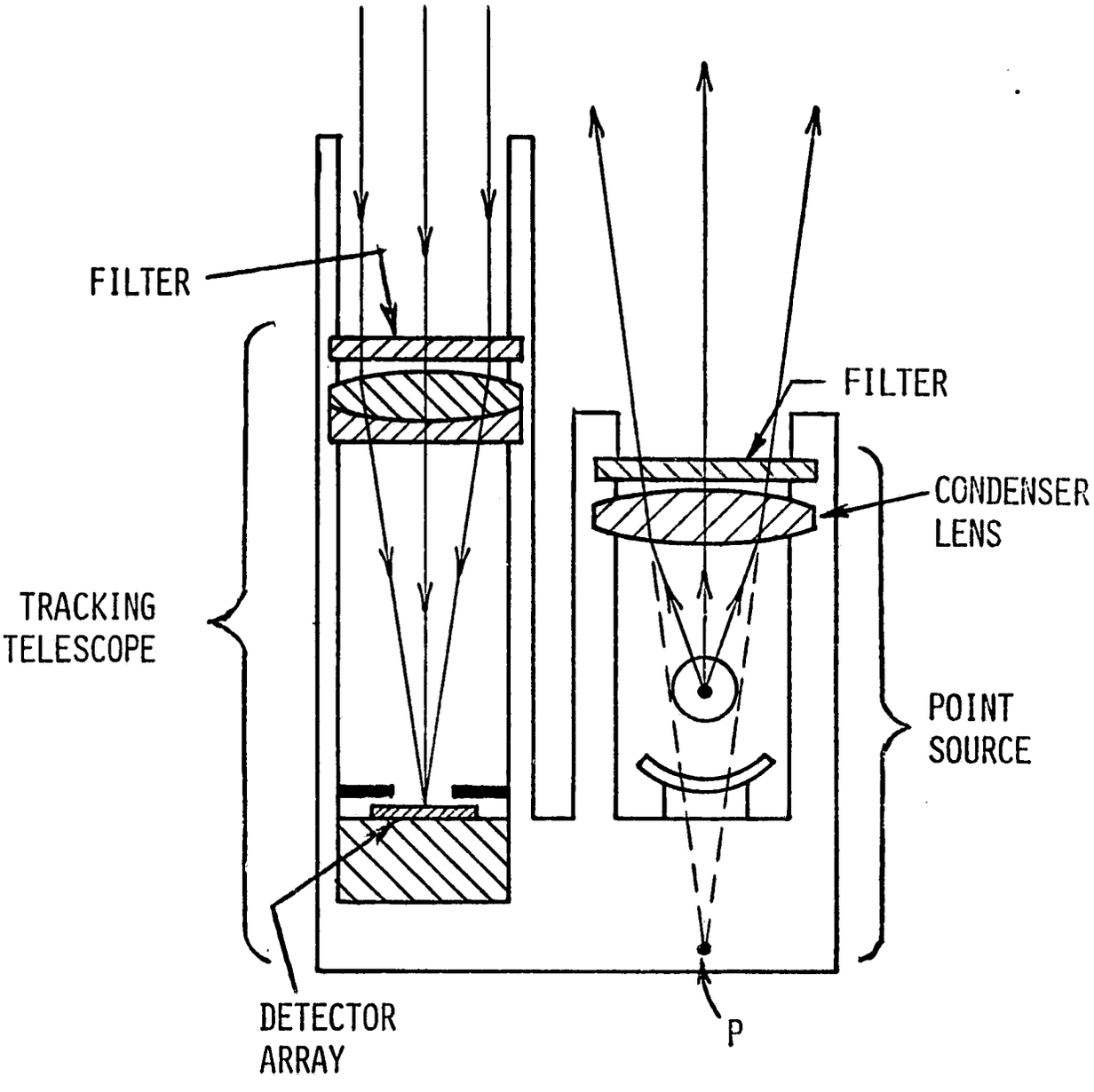
FILTER
FILTER
CONDENSER
LENS
TRACKING
TELESCOPE
POINT
SOURCE
DETECTOR
ARRAY
P

Figure 4.8

by the cube corner on an array-type detector. The purpose of the two bandpass filters is to attenuate point source radiation in spectral regions which might interfere with the White Light Coronagraph, and also to decrease the effects of stray light on the tracking telescope by, effectively, tuning it to the point source radiation.

Alternatively, the point source could be formed by focussing the beam of a small solid-state laser to a real or virtual point image. The angular divergence of the resulting point source would be equal to the laser beam diameter divided by the focal length of the focussing lens.

The occulter sensor data processing would be accomplished in real time using advanced microprocessors. The signals from the detector arrays would be clocked out and digitized. A threshold sensing algorithm would then identify by their signal levels those detector elements which probably lie within the area of the point source image, entering their locations and signal levels into memory. (This decreases the required memory capacity, since the output of the entire array does not have to be stored.) Those signals above the threshold which are not part of a cluster which would characterize this image will be discarded. The remaining signal levels will then be adjusted according to the measured sensativity of each given detector element, and the position of the centroid of the image will be computed. The positions of the centroids for both trackers will then be compared, and, allowing for the offsets programmed into the system during optical alignment, the pitch, yaw, and roll errors of the occulter will be calculated. Then, appropriate error signals will be generated for the pointing system.

4.7 Tracking Telescope Detector Array

There is a tradeoff between the angular resolution and the angular dynamic range (field of view) of the tracking telescope, assuming a detector array having a given number of elements. The tradeoff can be expressed as follows:

$$\tau = N\delta/k \qquad (4.3)$$

where:

τ = full field angle of the tracking telescope

N = linear number of elements in the detector array

δ = required angular resolution

k = interpolation constant (the fraction of a pixel spacing to which the centroid of the image can be determined).

For instance, let N=256, assuming a 256 x 256 detector array such as the Reticon RA-256x256. The most stringent angular resolution requirement on the occulter sensor from Table 4.1 will be to monitor the absolute orientation of $\vec{X}$ with respect to $\vec{S}$ to within 0.3 seconds. Since this requirement involves the Fine Sun Sensor as well as the Occulter Sensor(s), the angular resolution δ required of the Occulter Sensor(s) will have to be about 0.15 seconds. (The roll sensing requirement of 5 seconds RMS requires a δ of about 0.25 seconds, assuming that the cube corners are separated by about 1/10 of the boom length and that the angular sensing errors are equally divided between the two occulter sensors. Thus, the roll sensing requirement is less stringent). Interpolation constants in the range of 1/20 to 1/100 of a pixel can be obtained if the pattern noise of the detector array is cancelled out by a periodic uniform flooding the detector array, therby obtaining a relative calibration for each detector element. Assume a conservative value for k of 1/20. Then the resulting field of view τ from equation 4.3 is 0.21°. With the 62.5 micron pixel spacing of the Reticon RA-256x256 array, the required focal length for the Tracking Telescope must be (k/δ) x 62.5 microns or 430 cm. Thus, with this detector, the field of view is fairly small and the required focal length is quite large. However, the angular dynamic range could be increased by the use of coarse occulter sensors analogous to the coarse sun sensors for initial acquisition, and the length of the Tracking Telescope could be greatly decreased by the use of telephoto optics, such as a Cassegrain system. With a Cassegrain configuration, the 430 cm dimension could readily be decreased by a factor of 5 to 86 cm.

With the Reticon detector, the 0.05 arc second short term requirement for monitoring the relative motion of $\vec{X}$ with respect to $\vec{S}$ would correspond to decreasing the interpolation constant k from 1/20 to about 1/60. Since this is a relative rather than an absolute sensing requirement, which does not depend on accurate cross-calibration of the sensativity of detector elements, achieving a value for k of 1/60 is not unreasonable here.

The radiated power required from the point source is also quite reasonable. The saturation exposure level for the Reticon array is 0.25 μ watt sec/cm^2. Assume that the image of the point source should produce an exposure

level of 10% of saturation, or .025 μ watt sec/cm^2, and that the device is working at a frame rate of 0.05 seconds. Assume also that the beam diverging from the point source overfills a 5 cm diameter cube corner by a factor of 10^4 in area. The return power from the cube corner will be spread over an area twice the diameter of the cube corner, or 10 cm. With an aperture for the tracking telescope of 3 cm, about 1/10 of the return power will be intercepted by the Tracking Telescope Objective. This power will be spread over an image area about 10 arc seconds in diameter (or 3.4×10^{-4} cm^2 for an effective focal length of 430 cm.), assuming a diffraction-limited optical system. Assume a combined transmittance for the bandpass filters of 0.25. Then the required source power W is

$$W = (.025\ \mu\text{watts sec/cm}^2 \times 3.4 \times 10^{-4}\ \text{cm}^2 \times 10^4 \times 10)/(.05\ \text{sec} \times .25)$$

$$= .068\ \text{milliwatts} \qquad (4.4)$$

In order that the actual source size not appreciably increase the diffraction-limited size of the image, the angle subtended by the source must be small compared to 10 arc seconds. That is, it must be small compared to 4.8 mm for a 50 meter boom, and small compared to 1.0 mm for a 10 meter boom. At the low power levels required here, these restrictions should present no problems.

Thus, this type of occulter sensor appears to be feasible using existing detector arrays and sources of very modest power, although the field of view could be widened and the tracking telescopes shortened by using next-generation detector arrays having more elements and smaller pixel sizes.

APPENDICES

Appendix A: Program Listing for "SCATTER"

Appendix B: Calculation of the Earthshine Factor F

Appendix C: Location of Virtual Image Formed by a Cube Corner Reflector

Appendix A: Program Listing for "SCATTER"

```
      PROGRAM SCATTER(INPUT,OUTPUT,TAPE5=INPUT,TAPE6=OUTPUT)
C
C
C  THE FIRST PART OF THIS PROGRAM COMPUTES THE INTENSITY DISTRIBUTION
C    OF THE RADIATION DIFFRACTED BY AN EXTERNAL OCCULTING DISK INTO THE
C    ENTRANCE APERTURE OF A CORONAGRAPH, USING THE FORMULATION OF FORT,
C    MOREL, AND SPAAK IN ASTRONOMY AND ASTROPHYSICS 63,243 (1978).
C    THE SOURCE IS ASSUMED TO BE THE SUN, WITH AN ANGULAR RADIUS BETA
C    OF 16.0 ARC MIN OR 0.0046542 RADIANS.
C  WAVELENGTHS OF 5000A AND 1216A ARE USED IN THIS CALCULATION.
C
C  LINEAR UNITS ARE CM UNLESS OTHERWISE INDICATED.
C
C  Y=RADIAL DIST FROM OPTICAL AXIS IN THE PLANE OF CORONAGRAPH LENS.
C  D=DISK-TO-CORONAGRAPH DISTANCE.
C  RADISK=RADIUS OF OCCULTING DISK.
C  E1=CALCULATED INTENSITY OF THE DIFFRACTION PATTERN IN THE PLANE OF
C    THE CORONAGRAPH LENS VERSUS X AT 5000A. (E1 IS NORMALIZED TO THE
C    UNOCCULTED SOLAR INTENSITY).
C  E2=INTENSITY IN THE DIFFRACTION PATTERN AT 1216A.
C  XMAX=RADIUS OF THE UMBRA OF THE SHADOW OF THE DISK=(RADISK-(BETA*D))
C  DELTA=LINEAR DISTANCE MEASURED INWARD FROM THE EDGE OF THE UMBRA IN
C    THE PLANE OF THE CORONAGRAPH LENS.
C  THETA=ANGULAR DISTANCE MEASURED INWARD FROM THE EDGE OF THE UMBRA.
C
C
C
      D=1000.0
      DO 100 I=1,9
      D=D+1000.0
C  COMPUTE RADISK ASSUMING A CORONAGRAPH APERTURE OF 12.6 CM (1.0 ARC
C    SEC RESOLUTION AT 5000A) AND A MIN LIMB OBSERVING DISTANCE OF 0.10
C    SOLAR RADII.
      RADISK=6.30+(1.10*0.0046542*D)
      ALPHA1=(.00005)/(6.2832*RADISK)
      ALPHA2=(.000012161/(6.2832*RADISK)
      XMAX=RADISK-(.0046542*D)
      BETAD=.0046542*D
```

```
C  PRINT HEADINGS.
C     FORMAT 1000 LEAVES A SPACE.  FORMAT 1200 STARTS A NEW PAGE.
C     FORMAT 1100 PRINTS **********.
      WRITE(6,1200)
 1200 FORMAT(1H1)
      WRITE(6,1000)
 1000 FORMAT(1H0)
      WRITE(6,1100)
      WRITE(6,1100)
 1100 FORMAT(99H **********************************************************
     1**********************************************)
      WRITE(6,1000)
      DD=D/100.0
      WRITE(6,1300) DD,RADISK
 1300 FORMAT(2X*D=*,F5.1,*4 RADISK=*,F6.2,*CM  X    DELTA=   THETA   INT
     1ENSITY   INTENSITY     INTENSITY(5000A)/20*)
      WRITE(6,1400) XMAX
 1400 FORMAT(11X*XMAX=*,F6.2,*CM    (CM)  XMAX-X   (MIN)    (1216A)    (5
     1000A)*)
```

PROGRAM SCATTER 74/74 OPT=1 FTN 4.6+433E 11/09/79 16.59.39

```
      WRITE(6,1000)
      X=XMAX
  110 X=X-0.10
      GO TO 130
  120 X=X-0.50
  130 IF(X.LT.0.0) X=0.01
      C=1.0+1((RADISK-X)*(RADISK-X)-(DETAD*DETAD))/(2.0*RADISK*X))
      CC=SQRT(C*C-1.0)
      E1=(RADISK*ALPHA1)/(3.1416*.0346542*X*CC)
      E2=(E1*ALPHA2)/ALPHA1
      DELTA=XMAX-X
      THETA=(7437.75*DELTA)/D
      E20=E1/20.0
```

```
      WRITE(6,1500) X,DELTA,THETA,E2,E1,E20
 1500 FORMAT(25X,F6.2,F8.2, F9.2,1PE12.2,1PE12.2, 1PE17.2)
      IF(X.LT.0.010001) GO TO 100
      IF(DELTA.GE.2.0) GO TO 120
   75 GO TO 110
  100 CONTINUE
      WRITE(6,1000)
      WRITE(6,1100)
      WRITE(6,1100)
   80 WRITE(6,1100)
      WRITE(6,1100)
      WRITE(6,1200)
C
C  ***************************************************************
   85 C  ***************************************************************
C
C  THE SECOND PART OF THIS PROGRAM COMPUTES THE RELATIVE INTEGRATED
C    FLUX S DIFFRACTED INTO THE CORONAGRAPH LENS FOR VARIOUS VALUES
C    OF D, RADISK, AND CORONAGRAPH LENS RADIUS A.
   90 C  THIS CALCULATION ALSO FOLLOWS THAT OF FORT, MOREL, AND SPAAK.
C    S IS DEFINED AS THE INTEGRATED FLUX WITH THE EXTERNAL DISK IN PLACE
C        DIVIDED BY THAT WITHOUT THE DISK.
C    S1 AND S(5000A) ARE VALUES OF S FOR 5000A.
C    S2 AND S(1216A) ARE VALUES OF S FOR 1216A.
   95 C
C  DIST1=MINIMUM  LIMB OBSERVING DISTANCE, IN SOLAR RADII.
C  DIST2=DISTANCE TO CENTERLINE OF BLUR OF DISK, IN SOLAR RADII.
C  DIST3=DISTANCE FROM LIMB WHERE VIGNETTING CEASES, IN SOLAR RADII.
C
  100 C
      DO 400 K=1,3
      IF(K.EQ.1) A=6.3
      IF(K.EQ.2) A=3.15
      IF(K.EQ.3) A=12.6
  105 D=1000.0
      DO 500 J=1,10
      D=D+1000.0
      BETAD=.0046542*D
```

```
C  RMIN IS THE MIN VALUE OF RADISK.  COMPUTE RMIN TO GIVE A MIN LIMB
C    OBSERVING ANGLE OF 0.5 ARC MINUTES.
      RMIN =A+(.0046542*D)+(.00014544*D)
      APTURE=2.0*A
      DD=D/100.0
C  PRINT HEADINGS
```

PROGRAM SCATTER 74/74 OPT=1 FTN 4.6+433E 11/09/79 10.59.39

```
      WRITE(6,1200)
      WRITE(6,1000)
      WRITE(6,1100)
      WRITE(6,1100)
      WRITE(6,550)  APTURE,DD
  550 FORMAT(2X*APERT=*,F4.1,*CM  D=*,F5.1,*M  RADISK  MIN LIMB  MID BLU
     1P  FULL APERT   S(1216A)   S(5000A)   S(5000A)/20*)
      WRITE(6,560)
  560 FORMAT(                    27X*(CM)   DISTANCE  DISTANCE   DISTANCE
     1*)
      WRITE(6,1000)
C  INCREASE THE ANGULAR RADIUS OF RADISK IN INCREMENTS OF 0.10 ARC MIN
C    OVER A RANGE OF 7.50 ARC MIN.
      STEP=D*.000029089
      RADISK=RMIN-STEP
      DO 600 M=1,76
      RADISK=RADISK+STEP
      ALPHA1=(.00005)/(6.2832*RADISK)
      ALPHA2=(.00001216)/(6.2832*RADISK)
      SHATA= (RADISK-BETAD) *(RADISK-BETAD)
      SO= 1.0+(SHATA/(2.0 *RADISK*BETAD))
      SIGHO= ALOG(SO+ SQRT(SO*SO-1.0))
      SA= 1.0+((SHATA-A*A)/ (2.0*RADISK*BETAD))
```

```
                SIGHA= ALOG(SA +SQRT(SA*SA-1.0))
                DIFF= SIGH0-SIGHA
140             S1= (2.0*RADISK*RADISK*ALPHA1* DIFF)/(3.1416* A*A* .00465421
                S2= (S1*ALPHA2)/ ALPHA1
                S20= S1/20.0
                DIST1= 214.859*(((RADISK-A) /D) -.00465421
                DIST2= 214.859*(( RADISK/D) -.00465421
145             DIST3= 214.959*(((RADISK+A) /D) -.00465421
                WRITE(6,650)  RADISK, DIST1,DIST2,DIST3, S2,S1, S20
            650 FORMAT(26X,  F5.1, F9.3, F11.3,F10.3, 1PE14.2, 1PE11.2,1PE12.2)
            600 CONTINUE
            500 CONTINUE
150         400 CONTINUE
                WRITE(6,1000)
                WRITE(6,1100)
                WRITE(6,1100)
                WRITE(6,1100)
155             STOP
                END
```

Appendix B: Calculation of the Earthshine Factor F

The power received by a surface (e.g., the occulting disk) in earth orbit due to earthshine is estimated as follows. The revelant geometry is shown in Figure 5.1, with the earth represented as a sphere of radius r. The disk is at an altitude H above the surface and is assumed to be oriented normally to the line joining the sub-earth point. The solar direction is in the y-z plane at an arbitrary angle ψ with respect to the y-axis. The power per unit area received by the disk from a surface element dA on the earth is

$$dP = \frac{I(\theta,\phi)\, dA\, S(\gamma)\alpha\cos\beta}{D^2} \qquad (5.1)$$

where $I(\theta,\phi)$ is the power per unit area received from the sun by a surface element located at θ and ϕ. The angles θ and ϕ are the usual spherical polar coordinates and the Z axis is the radial direction containing the occulting disk. The quantity α is the earth's albedo which we define to be the ratio of power radiated back into space to the power received by a given surface element. For simplicity, we assume that α is independent of position on the earth and the angle of incidence of the solar flux. We further define a function $S(\gamma)$ to be the atmospheric scattering law which, for simplicity, we take to be a Lambertian scatterer, independent of the angle of incidence of the solar flux (i.e., $S(\gamma) = \cos(\gamma)/\pi$). The angle between the scattering direction and the local radial direction is γ.

The total power received per unit area of the disk is then

$$P = \iint_{\substack{\text{Sunlit}\\ \text{Hemisphere}}} \frac{I(\theta,\phi)S(\gamma)\ \alpha\ \cos\beta\ r^2\ \sin\theta d\theta d\phi}{D^2} \qquad (5.2)$$

where $I(\theta,\phi)$ can be shown to be

$$I(\theta,\phi) = I_0\ (\cos\psi\cos\theta + \sin\psi\sin\theta\sin\phi), \qquad (5.3)$$

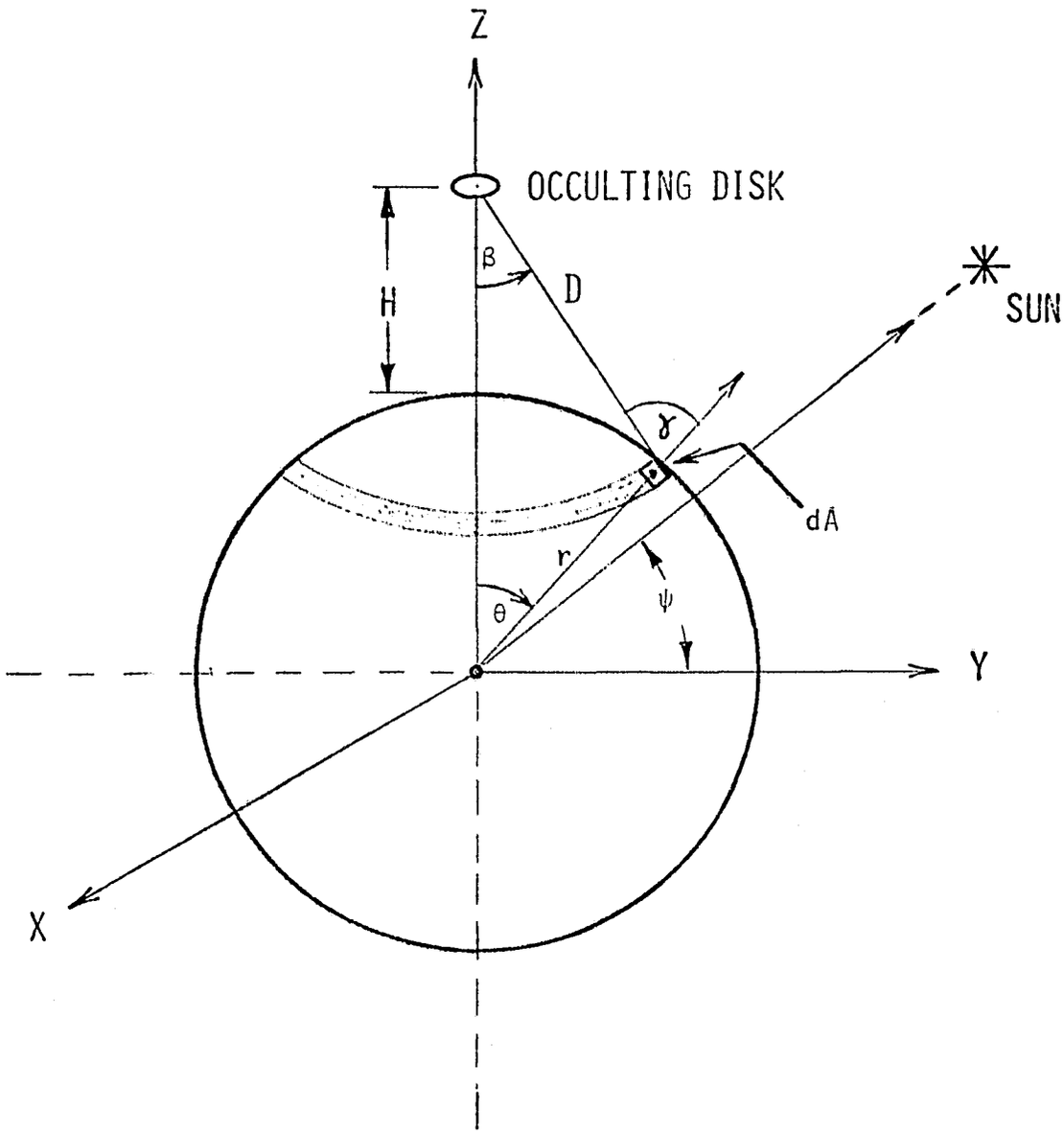

Figure 5.1

on the sunlit hemisphere. The integral given by equation (5.2) is somewhat difficult to carry out except for the cases where $\psi=0°$ and $\psi=90°$. For these two cases we find

$$P_{\psi=0} = 2\alpha I_0 \int_0^{\theta_c} \frac{\cos\theta \sin\theta \cos\gamma \cos\beta \, r^2 \, d\theta}{D^2} \qquad (5.4)$$

and

$$P_{\psi=90°} = \frac{2\alpha I_0}{\pi} \int_0^{\theta_c} \frac{\sin^2\theta \cos\gamma \cos\beta \, r^2 \, d\theta}{D^2} \qquad (5.5)$$

where the variables D, β and γ are functions only of θ and of the constants of the problem (e.g., r and H). Here, θ_c corresponds to the tangent point.

The two integrals 5.4 and 5.5 have been carried out numerically and the results, expressed as the dimensionless Factor F (equal to $P/\alpha I_0$), are shown in Figures 3.5 and 3.7.

Appendix C: Location of the Virtual Image Formed by a Cube Corner Reflector

Given:

1. A Theorem from geometric optics:

   If L is a line normal to a plane mirror M passing through a point P which is located a distance d from plane M, then the virtual image of P lies on the opposite side of M on the same line L, and is also located a distance d from M.

2. A point light source P located at coordinates $(+x_o, +y_o, +z_o)$.

3. A cube corner reflector made up of three mutually perpendicular mirrors M_x, M_y, and M_z whose lines of intersection lie along the x, y, and z axes, as shown in Figure 5.2.

Then:

1. After reflection from Mirror M_x, the virtual image P' of P will lie at the coordinates $(-x_o, +y_o, +z_o)$, by the above Theorem.

2. After an additional reflection from M_y, the virtual image P'' will lie at the coordinates $(-x_o, -y_o, +z_o)$, by the above Theorem.

3. After the final reflection from M_z, the virtual image P''' will lie at the coordinates $(-x_o, -y_o, -z_o)$, by the above Theorem.

Conclusion:

After three reflections within the cube corner, the source P, the vertex point of the corner cube, and the final virtual image P''' will be equally spaced along the same straight line l.

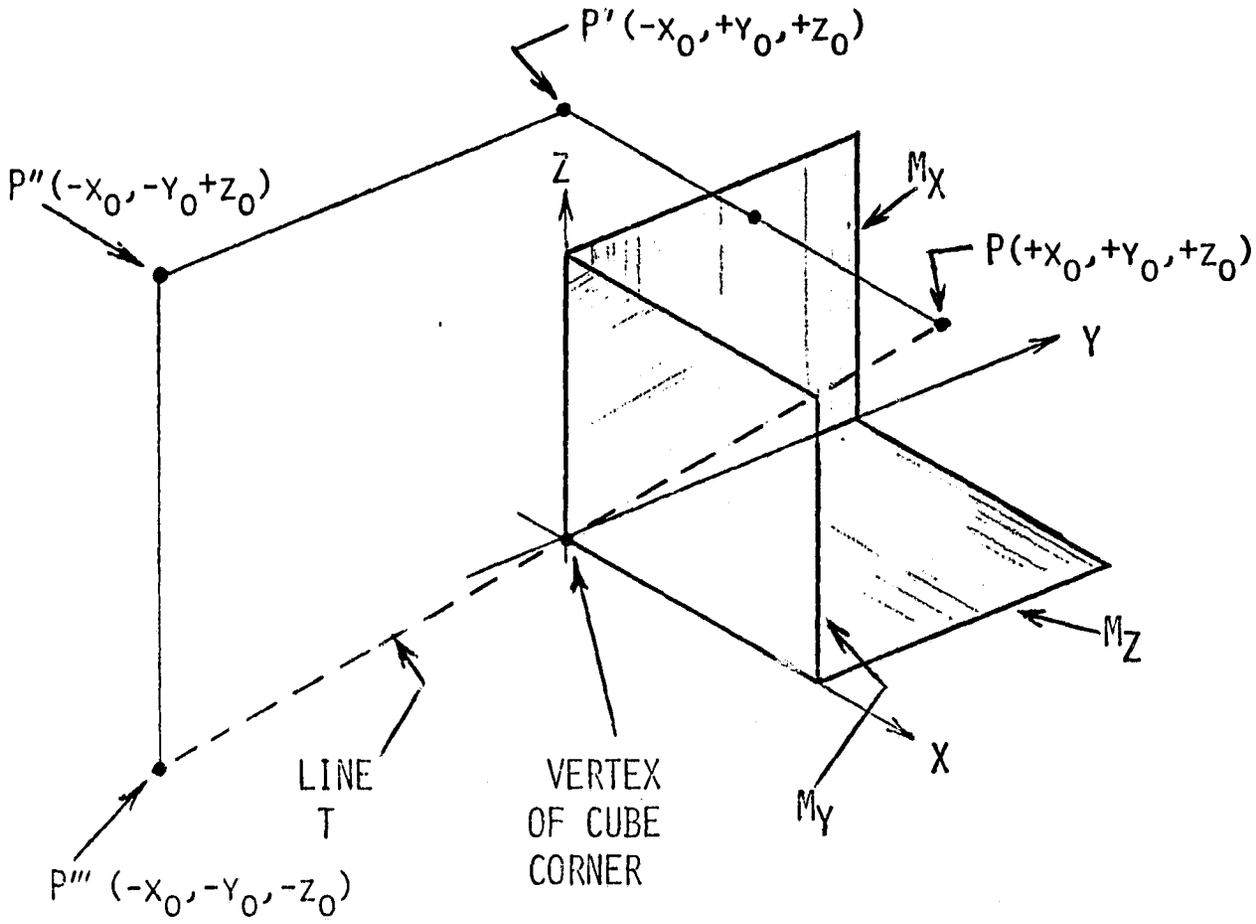
P'(-X0,+Y0,+Z0)
P''(-X0,-Y0+Z0)
Z
MX
P(+X0,+Y0,+Z0)
Y
MZ
X
MY
LINE
T
VERTEX
OF CUBE
CORNER
P''' (-X0,-Y0,-Z0)

Figure 5.2